Peer reviewed version

Link to published version (if available):
[10.1126/scitranslmed.aav5055](#)

Link to publication record in Explore Bristol Research
PDF-document

University of Bristol - Explore Bristol Research
General rights

Adipose tissue-derived WNT5A regulates vascular redox signaling in obesity via USP17//RAC1-mediated activation of NADPH oxidases

Ioannis Akoumianakis[1]*, Fabio Sanna[1]*, Marios Margaritis[1], Ileana Badi[1], Nadia Akawi[1], Laura Herdman[1], Patricia Coutinho[1], Harry Fagan[1], Alexios S Antonopoulos[1], Evangelos K Oikonomou[1], Sheena Thomas[1], Amy P Chiu[1], Surawee Chuaiphichai[1], Christos P Kotanidis[1], Constantinos Christodoulides[3], Mario Petrou[2], George Krasopoulos[2], Rana Sayeed[2], Lei Lv[1], Ashley Hale[1], Meisam Naeimi Kararoudi[1], Eileen McNeill[1], Gillian Douglas[1], Sarah George[4], Dimitris Tousoulis[5], Keith M Channon[1], Charalambos Antoniades[1]‡

[1]Division of Cardiovascular Medicine, University of Oxford, Oxford, OX3 9DU, UK

[2]Department of Cardiothoracic Surgery, Oxford University Hospitals NHS Trust, Oxford, OX3 9DU, UK

[3]Oxford Centre for Diabetes, Endocrinology and Metabolism, University of Oxford, Oxford, OX3 7LE, UK

[4]Bristol Medical School, Research Floor Level 7, Bristol Royal Infirmary, Bristol, BS2 8HW, UK

[5]Cardiology Department, Athens University Medical School, Athens, 115 27, Greece

*These authors contributed equally to the study

‡Corresponding author. E-mail: antoniad@well.ox.ac.uk

One sentence summary: Adipose tissue-secreted WNT5A triggers vascular disease in obesity by activating migration of vascular smooth muscle cells, via a USP17/Rac1/NADPH oxidases-dependent mechanism.

OVERLINE: CARDIOMETABOLIC DISEASE

Abstract

Obesity is associated with changes in the secretome of adipose tissue (AT), which affects the vasculature through endocrine and paracrine mechanisms. Wingless-related integration site 5A(WNT5A) and secreted frizzled related protein 5 (SFRP5), adipokines that regulate non-canonical Wnt signaling, are dysregulated in obesity. We hypothesised that WNT5A released from AT exerts endocrine and paracrine effects on the arterial wall through non-canonical RAC1-mediated Wnt signaling. In a cohort of 1,004 humans with atherosclerosis, obesity was associated with increased WNT5A bioavailability in the circulation and the AT, higher expression of WNT5A receptors Frizzled 2 and 5 in the human arterial wall, and increased vascular oxidative stress due to activation of NADPH oxidases. Plasma concentration of WNT5A was elevated in patients with coronary artery disease compared to matched controls and was independently associated with calcified coronary plaque progression. We further demonstrated that WNT5A induces arterial oxidative stress and redox-sensitive migration of vascular smooth muscle cells via Frizzled 2-mediated activation of a previously uncharacterised pathway involving the deubiquitinating enzyme ubiquitin-specific protease 17 (USP17) and the GTPase RAC1. Our study identifies WNT5A and its downstream vascular signaling as a link between obesity and vascular disease pathogenesis, with translational implications in humans.

Introduction

Evidence suggests that obesity is closely related to vascular disease (*1*). However, the described U-shaped association between body mass index (BMI) and mortality(*2*) indicates the need for better understanding of the links between adipose tissue (AT) biology and vascular

(patho)physiology in order to develop therapeutic strategies to prevent the vascular complications of obesity.

AT is a dynamic organ with regional biological variability (*3*), secreting a wide range of adipocytokines with vascular effects (*4, 5*). Perivascular AT (PVAT) exerts paracrine effects on the vascular wall, whereas "remote" AT depots such as subcutaneous (ScAT) and thoracic AT (ThAT) exert endocrine effects by enriching the circulating adipocytokine pool. Recent evidence suggests that obesity is associated with a shift of the AT secretome from vasoprotective/anti-atherogenic to a pro-atherogenic phenotype (*6*).

Redox signaling is central to vascular disease, exerting multiple cytotoxic and pro-inflammatory effects (*7*). NADPH oxidases (NOX) are major sources of vascular reactive oxygen species (ROS), and the activity of some NOX isoforms (namely NOX 1 and NOX 2) is dependent on the GTPase RAC1(*8*). In turn, ROS regulate the migration of vascular smooth muscle cells (VSMCs) to the intima layer of the vascular wall, which is involved in vascular disease processes such as atherosclerotic plaque formation (*9*). However, the mechanisms by which obesity affects vascular redox signaling are unclear.

The wingless-related integration site (Wnt) signaling pathway is activated by a family of Wnt glycoprotein ligands consisting of 19 members in humans (*10*) and is negatively regulated by secreted frizzled related proteins (Sfrp), which act as decoy receptors for Wnt ligands (*11*). Downstream Wnt signaling is mediated by the canonical pathway, which involves β-catenin and is triggered by WNT3 (*10*), and the non-canonical pathways, which do not involve β-catenin and are triggered by WNT5A and WNT11(*12, 13*). Despite the established role of non-canonical Wnt signaling in cancer biology, its role in vascular disease pathogenesis in the context of obesity is unknown.

Recent work suggests that AT secretes WNT5A and SFRP5(*14*), molecules with potential vascular effects (*15*). Imbalance in the AT production of WNT5A and SFRP5 in obesity may result in a 'vicious cycle' of increased AT inflammation and insulin resistance (*14*), indirectly triggering vascular complications of obesity. However, the potential role of AT-derived WNT5A and SFRP5as direct mediators of atherogenesis in obesity has not been investigated so far. We hypothesised that dysregulated AT secretion of WNT5A and SFRP5may lead to altered endocrine and paracrine effects on the vascular wall in obesity. We further explored the potential links between AT-derived WNT5A and the mechanisms of vascular disease pathogenesis.

Results

Wnt ligand expression profile in adipose tissue depots from patients with atherosclerosis

We first explored the gene expression profile of all 19 Wnt ligands in human PVAT, ThAT and ScAT. *WNT5A* was the most highly expressed Wnt ligand in PVAT (Fig. 1A), whereas *WNT11* was the most highly expressed Wnt ligand in ThAT and ScAT, with *WNT5A* still being among the four most highly expressed Wnt ligands in these depots (Fig. 1, B and C). As both WNT5A and WNT11 are known to be non-canonical Wnt signaling pathway activators, and considering that WNT5A is the most abundant PVAT-derived paracrine ligand of the two, we focused on the potential role of WNT5A as a mediator of the vascular complications of obesity via non-canonical Wnt signaling.

WNT5A and SFRP5adipose gene expression profiles in obesity

Plasma WNT5A was significantly increased in obese humans (Fig. 1D), accompanied by reduced plasma concentration of its antagonist SFRP5 (Figure 1E). We then focused on evaluating the WNT5A/SFRP5 ratio(*16*), since this is regarded as a more accurate integrated indication of overall Wnt signaling balance compared to evaluating WNT5A and SFRP5concentrations individually. We observed a strong positive correlation between BMI and plasma WNT5A/SFRP5 ratio (Figure 1F). Consistently, there was a positive association between BMI and the gene expression of *WNT5A*/*SFRP5* in human ThAT (Fig. 1, G-I), but not in human ScAT (fig. S1, A-C). This suggests that increased *WNT5A*/*SFRP5* gene expression in visceral adiposity (ThAT) could be linked with obesity-related vascular disease in humans.

Interactions between obesity, WNT5A/SFRP5 and vascular disease

We next explored the associations between obesity, WNT5A/SFRP5, and markers of vascular disease. Although obesity was not associated with the gene expression of *WNT5A* (Figure 2A), *SFRP5* (Figure 2B), or the *WNT5A/SFRP5* ratio in human IMAs (Figure 2C), it was linked with significantly altered gene expression of *WNT5A* and *SFRP5*in human PVAT. PVAT from obese/morbidly obese patients expressed significantly more *WNT5A* (Figure 2D), less *SFRP5* (Figure 2E), and thus had a higher *WNT5A/SFRP5* ratio compared to lean counterparts (Figure 2F). Obesity was related to a significant increase in the gene expression of WNT5A receptors Frizzled 2 (*FZD2*) (Figure 2G) and Frizzled 5 (*FZD5*) (Figure 2H) but not receptor tyrosine kinase-like orphan receptor 1 (*ROR1*) (Figure 2I) in human IMAs. This suggests that, in obese humans, arteries display increased sensitivity to the consequences of Wnt signaling, which may be a mechanistic link to the increase in arterial oxidative stress observed in obesity.

To evaluate the association between the WNT5A/SFRP5 ratio and coronary artery disease (CAD) in humans, we designed a case-control study (study 2) in which 70 patients with CAD

were matched for age, gender, and BMI with 70 controls without obstructive CAD [confirmed by computed tomography (CT) angiography as having no coronary plaque causing>50% luminal stenosis]. Patients with CAD hadhigher plasma WNT5A (Figure 2J), lower SFRP5 (Figure 2K), and a higher plasma WNT5A/SFRP5 ratio (Figure 2L) compared to controls. The presence of CAD was associated with circulating WNT5A (Bstand = 0.23, P = 0.00), SFRP5 (Bstand = - 0.21, P = 0.00) and their ratio (Bstand = 0.21, P = 0.00) independently of traditional risk factors that differed significantly between the two cohorts of study 2 (Figure 2M). WNT5A/SFRP5 and all cardiovascular risk factors (hypertension, hyperlipidaemia, diabetes, and smoking) were associated with the presence of CAD by univariate analysis (table S1). However, in a multivariable model that included WNT5A/SFRP5 and all risk factors, only hypertension and hyperlipidaemia remained independently associated with CAD, independently from each other (Fig. 2M).

To explore the potential value of WNT5A as a surrogate biomarker of vascular disease progression in humans, we designed a validation study (study 3) that involved individuals scanned by non-contrast CT at two different time points, 3-5 years apart, for evaluation of coronary calcified plaque burden. In 68 individuals studied, plasma WNT5A concentration was significantly elevated in patients that demonstrated calcified plaque progression, defined as a difference in coronary calcium score (CCS) ≥1 (n=32) (Figure 2N; baseline CCS: 0.00[0.00-76.70] and follow-up CCS: 15.63[0.00-182.88] presented as median [25th-75th percentile] in the entire study 3; differences in CCS between baseline and follow-up (ΔCSS) are further presented in Fig. 2N for each group)). Similarly, in 38 patients with baseline CCS=0, plasma WNT5A was positively associated with the development of new calcification (follow-up CCS: 0.00[0.00-6.93] presented as median [25th-75th percentile] in the entire study arm; follow-up CCS values in the new onset calcification group are also further presented in Fig. 2O). Upon multivariate regression analysis, plasma WNT5A was associated with progression of

calcification (Bstand=0.242, P=0.047) and new onset calcification (Bstand=0.367, P=0.03) independently of age and sex (table S3).

WNT5A/SFRP5 as regulators of redox state in the human arterial wall

We observed that BMI was not only associated with increased circulating and AT WNT5A/SFRP5 ratio but also with higher basal (Figure 3A) and NADPH-stimulated (Figure 3B) superoxide ($O_2.-$) generation in human internal mammary artery (IMA) segments. To examine whether the WNT5A/SFRP5 balance could alter human arterial redox state and thus be a mechanistic link between obesity and oxidative stress, we next explored the interactions between $O_2.-$ generation in human IMAs and WNT5A/SFRP5 ratio in plasma and PVAT from the patients in study 1. High plasma WNT5A/ SFRP5 ratio as well as high *WNT5A/ SFRP5* expression in PVAT were related with higher basal and NADPH-stimulated $O_2.-$ production in human IMAs (Figures 3C-F), whereas arterial *WNT5A/SFRP5* gene expression was not associated with arterial redox state (Figure 3G-H). Since endogenous *WNT5A* gene expression in the human IMA is negligible compared to that in PVAT (fig. S1D), we hypothesised that the effects of WNT5A on the arterial wall are endocrine (resulting from its increased concentration in the circulation and reaching the endothelium and VSMCs via the lumen and vasa vasorum for large arteries) and paracrine (reaching the VSMCs and the endothelium via diffusion from the PVAT) rather than autocrine.

To understand whether the association between obesity and NADPH oxidase activity in human arteries is dependent on the *WNT5A/SFRP5* ratio in PVAT, we performed multivariate analysis in which arterial NADPH-stimulated $O_2.-$ was used as dependent variable, and obesity classification, diabetes, smoking, sex and age were used as independent variables. In the presence of *WNT5A/SFRP5* gene expression in PVAT, in the model, obesity was not a

significant predictor of arterial NADPH-stimulated $O_2 \cdot^-$, suggesting that the effects of obesity on human arterial redox state are WNT5A-dependent (table S4).

To explore whether the associations between WNT5A/SFRP5 and human vascular redox state are causal, we used *ex vivo* models of human IMAs (study 4), whereby serial IMA rings were incubated with WNT5A (100 ng/ml), SFRP5 (300 ng/ml), or the combination of the two factors for 45 minutes, and $O_2 \cdot^-$ generation was evaluated using lucigenin chemiluminescence and confirmed with dihydroethidium (DHE) staining. The concentration of WNT5A selected was near the maximum of the physiological levels of plasma WNT5A in patients of study 1 (range: 1-112 ng/ml). WNT5A induced a 4-fold increase in arterial basal $O_2 \cdot^-$, an effect prevented by co-incubation with SFRP5 (Figure 3I). Similarly, NADPH-stimulated $O_2 \cdot^-$ was increased (>2-fold) by WNT5A incubation, an effect prevented by SFRP5 (Figure 3J), and the same was observed when measuring the signal inhibited by the pan-NOX inhibitor Vas2870 (Figure 3K).

The specificity of the signal and the structural $O_2 \cdot^-$ localization within the human arterial wall were examined using DHE staining of human IMAs. Incubation of human IMAs with WNT5A for 45 minutes increased $O_2 \cdot^-$ generation, mainly from the VSMCs layer, an effect partially attenuated by SFRP5 and completely reversed by Vas2870 (Figure 3L), confirming that the effect was dependent upon NADPH oxidases. To examine whether the consequences of WNT5A on vascular redox state are dependent on the activation of NADPH oxidases, we explored its effects on vascular $O_2 \cdot^-$ after pre-incubation of human arteries with Vas2870. In the presence of Vas2870, WNT5A failed to increase vascular $O_2 \cdot^-$, confirming the central role of NADPH oxidases on the WNT5A -induced increase in vascular oxidative stress (Figure 3M-N). However, WNT5A did not affect the expression of any of the NOX isoforms (NOX1, NOX2, NOX4, or NOX5, fig. S2). In addition, plasma WNT5A/SFRP5 was not correlated with the expression of NOX2, NOX4 or NOX5 (fig. S3).

WNT5A also reduced nitric oxide (NO) bioavailability in human vessels [evaluated by *ex vivo* vasorelaxation in response to Acetylcholine (ACh)], an effect reversed by SFRP5 (fig. S4). WNT5A had no effect on the endothelium-independent responses to the NO donor sodium nitroprusside (SNP). To understand the underlying mechanism, we explored the effect of WNT5A on endothelial nitric oxide synthase (eNOS) coupling. WNT5A induced eNOS uncoupling in human arteries, demonstrated by increased LNAME-inhibitable $O_2^{.-}$, an effect reversed by SFRP5 (fig. S4). WNT5A promoted eNOS uncoupling by inducing the oxidation of eNOS co-factor tetrahydrobiopterin (BH4) without affecting the biopterin biosynthetic pathway (no modification of total vascular biopterin content, fig. S4). These data identify WNT5A as a regulator of vascular redox state that induces global changes in vascular redox signaling, influencing both VSMCs and the endothelium.

To further determine the causal effects of WNT5A on vascular NADPH oxidases activity in vivo, we used a doxycycline-inducible TetO mouse model (*Wnt5a +/rtTA+* mice) to induce global overexpression of *Wnt5a*. Treatment of *Wnt5a+/rtTA+* mice with doxycycline induced marked overexpression of *Wnt5a* in multiple tissues (fig. S5) resulting in increased plasma WNT5A compared to doxycycline-treated *Wnt5a–/rtTA+* littermate controls (Fig. 3O). *Wnt5a+/rtTA+* mice demonstrated higher basal, NADPH-stimulated, and Vas2870-inhibitable aortic $O_2^{.-}$ generation (Fig. 3P-R) compared to *Wnt5a–/rtTA+* controls, confirming that in vivo overexpression of WNT5A leads to activation of arterial NADPH oxidases.

Investigating the mechanism of WNT5A -induced arterial NADPH oxidases activation, we found that WNT5A activated the non-canonical planar cell polarity (PCP) Wnt signaling pathway, documented by c-Jun N-terminal kinase (JNK) phosphorylation (an established surrogate marker of PCP activation) in human IMAs as well as in the aortas of *Wnt5a+/rtTA+*

mice (Fig. 4, A and B, respectively). WNT5A induced RAC1activation (Figure 4C) in human arteries, leading to membrane translocation of RAC1and P47$_{phox}$ subunits of NADPH oxidases (Fig. 4D and E), which are crucial for the activation of the NOX1 and NOX2 isoforms of NADPH oxidases. The key role of RAC1 in the WNT5A -mediated NADPH oxidases activation was shown by demonstrating that the specific RAC1inhibitor NSC23766 prevented the WNT5A -induced increase of basal, NADPH-stimulated, and Vas2870-inhibitable O$_{2.-}$ in human IMAs (Figures 4F-H) and the aortas of *Wnt5a+/rtTA+* mice (Fig. 4I-K).

Adipocyte-derived WNT5A as a paracrine regulator of redox state in human VSMCs

To explore whether adipocyte- derived WNT5A can exert paracrine effects that control the redox state in the neighboring VSMCs, we first confirmed that recombinant WNT5A activates the PCP pathway (JNK-phosphorylation) and activates RAC1in primary human VSMCs in culture (fig. S6, Fig. 5, A and B) similarly to intact vessels. We confirmed that a physiological concentration of WNT5A (100 ng/mL) did not activate the canonical Wnt signaling pathway (evaluated by quantifying active beta catenin), in contrast to supra-physiological WNT5A concentrations (400 ng/ml), which activated canonical Wnt signaling (Fig. 5C). Incubation with WNT5A (100 ng/mL) increased basal, NADPH-stimulated, and Vas2870-inhibitable O$_{2.-}$ in VSMCs (Fig. 5D-F), suggesting that the effects observed at the level of whole vessel are largely driven by direct effects of WNT5A on VSMCs. We next used immortalized primary human preadipocytes endogenously expressing and secreting WNT5A and knocked down *WNT5A* using shRNA (Fig. 5G). We observed a significant reduction in basal VSMC O$_{2.-}$ when VSMCs were co-cultured with WNT5A -knockout (KO) adipocytes compared to sham control adipocytes (Fig. 5H). This reduction was due to a specific effect on the NOX2 isoform of

NADPH oxidase in VSMCs, as confirmed by significant reduction in gp91-dstat-inhibitable $O_2.-$ (gp91-dstat is a specific NOX2 inhibitor, Fig. 5I).

To further understand how WNT5A exerts its effects on human VSMCs in obesity, we knocked-down *FZD2* and *FZD5* (two receptors upregulated in arteries of obese humans) in VSMCs using siRNA (Fig. 6A-C). Down-regulation of *FZD2* was ~96%, and prevented the WNT5A -induced increase of basal, NADPH-stimulated, and Vas2870-inhibitable $O_2.-$ in human VSMCs (Fig. 6D-F). Knocking down *FZD5* was less efficient in this model, with ~65% reduction of the gene expression in human VSMCs, and was related with a moderate reduction of the WNT5A-induced increase of basal (Fig. 6G) but not NADPH-stimulated (Fig. 6H) or Vas2870-inhibitable (Fig. 6I) $O_2.-$.

Effects of WNT5A on human VSMC migration

To better understand the cellular effects of WNT5A signaling on VSMC biology and the contribution of redox signaling in this context, we incubated human VSMCs with WNT5A (100 ng/ml) in the presence or absence of pegylated superoxide dismutase (peg-SOD, 100 IU/mL), a scavenger of $O_2.-$, and performed microarray analysis to evaluate the differential gene expression profile induced by WNT5A compared to non-treated controls. WNT5A altered the expression of 1,890 differentially expressed genes (DEGs), of which 1,057 genes were upregulated and 833 were down regulated (fig. S7A).

The protein products of a substantial number of these DEGs were implicated in signal transduction pathways controlling cell growth, cell division, cell death, cell fate, and cell motility (fig. S6B). Functional annotation using Gene Ontology (GO) database showed that 135 of these DEGs were involved in cell motility, acting through pathways known to regulate

cell migration (Fig. 7, A-B). Thus, we hypothesised that WNT5A could influence the migration of primary human VSMCs.

We exposed human VSMCs to WNT5A (100 ng/ml) in the presence or absence of SFRP5 (300 ng/ml) and investigated changes in the ability of these cells to migrate using wound healing (fig. S7, C-D) and Boyden chamber (Fig. 7C) assays. WNT5A increased the migration of human VSMCs in a SFRP5-reversible manner (Fig. 7C-D), without affecting their proliferation (Fig. 7E). WNT5A could also induce a phenotypic switch of VSMCs, characterised by loss of contractile phenotype markers ACTA2 (actin α2, smooth muscle) and TGLN (trasngelin, or smooth muscle protein 22α, SM22α) and increased ratio of metalloproteinase 9 (MMP9) to MMP inhibitors TIMP1 and TIMP2 (fig. S8).

Ubiquitin-specific protease 17 (USP17) as a downstream mediator of WNT5A -mediated redox signaling

To determine the contribution of redox signaling to WNT5A -induced VSMC migration, we incubated primary human VSMCs with WNT5A in the presence or absence of peg-SOD. Peg-SOD prevented the WNT5A -induced changes in VSMC migration (Fig. 8A), suggesting that the changes in intracellular redox state described previously at least partially mediate the pro-migratory effects of WNT5A. Microarray results revealed that the effect of WNT5A on 28 of the previously described migration-related DEGs was reversed (at least partly) by peg-SOD, highlighting the DEGs as potential redox-sensitive genes (Fig. 8B).

The maximally differentially regulated (upregulated) gene in response to WNT5A was USP17, a member of a deubiquitinating enzyme multigene family within a tandemly repeated sequence (*17*) (Figure 8B and fig. S9A). VSMCs isolated from 10 patients were subjected to in vitro

WNT5A treatment with or without peg-SOD, and quantitative real time polymerase chain reaction (q-RT-PCR) confirmed that WNT5A increases the expression of USP17 (Figure 8C). USP17 was previously found to be involved in the activation of small GTPases (*18*) and to regulate cell motility (fig. S6).

To address the mechanistic role of USP17 in WNT5A -mediated RAC1activation, we knocked down USP17 using shRNA in HeLa cells (fig. S9B) and treated these cells with WNT5A (100ng/mL). WNT5A failed to induce persistent RAC1activation in USP17-KO HeLa cells as opposed to empty vector control cells (Fig. 8D). These data support the role of USP17 as a mediator of WNT5A -induced RAC1activation and RAC1-mediated redox signaling, identifying a potential therapeutic target.

Discussion

We demonstrate that obesity leads to an imbalance between WNT5A and SFRP5expression in PVAT and other adipose tissue depots such as ThAT, as well as alterations in circulating plasma concentrations in human vascular disease. We show that obesity is associated with upregulation of WNT5A receptors Fzd2 and Fzd5, which are involved in non-canonical Wnt signaling in human arteries. WNT5A secreted by human adipocytes enhances arterial NADPH oxidases activity, increasing $O_{2.-}$ generation and inducing endothelial dysfunction and eNOS uncoupling. This $O_{2.-}$ excess (by both and NADPH oxidases and, secondarily, uncoupled eNOS) induces redox-driven migration in VSMCs via USP17/ RAC1 activation, which may explain the clinical association of WNT5A with vascular disease. Patients with high plasma WNT5A were at higher risk for calcified plaque progression and new-onset coronary calcification. This work identifies WNT5A, its balance with SFRP5, and its receptors and downstream signaling network as mechanistic links between obesity and vascular

complications in humans, and as a potential therapeutic target for the prevention and treatment of such complications.

AT tissue biology displays remarkable regional variability and is dysregulated in obesity (*19*). Several studies have documented the biological discrepancy between visceral and superficial AT (*20*) and identified inflamed visceral AT as a source of adipocytokines with detrimental paracrine and endocrine effects on the vasculature (*5*). Previous studies have shown that WNT5A is expressed in the human adipose tissue (*21*), and have suggested that the balance between WNT5A and its decoy inhibitor SFRP5 may be involved in the pathogenesis of obesity and diabetes (*21*). We hypothesised that WNT5A and SFRP5 secretion from dysfunctional adipose tissue could play a role in the development of vascular disease in obesity.

After observing that WNT5A was the most abundant Wnt ligand expressed in the human PVAT, we confirmed that obesity was associated high WNT5A and low SFRP5plasma concentrations in patients with CAD. We observed a similar shift of the *WNT5A/SFRP5* gene expression ratio in ThAT and PVAT surrounding the IMA. It is therefore likely that increased WNT5A release from these visceral AT depots -- as well as the overall increased mass of these adipose tissue depots in obesity -- contributes to the obesity-related increase in plasma WNT5A. Obesity not only increased the exposure of the human arteries to high circulating WNT5A/ low SFRP5 (inside-to-outside vascular effects, from the lumen to the vascular wall) and high *WNT5A /* low *SFRP5*from PVAT (outside-to-inside vascular effects, from PVAT to the vascular wall), but it also led to upregulation of WNT5A receptors Fzd2 and Fzd5 in the human arterial wall. These receptors increased arterial sensitivity to non-canonical Wnt signaling. The combination of increased plasma WNT5A, together with the increased release of WNT5A from PVAT, drives the endocrine and paracrine effects, respectively, of adipose tissue-derived WNT5A on the human vascular wall. In a second nested case-control study, we showed a striking increase of plasma WNT5A accompanied by reduced circulating Sfpr5 in

patients with CAD compared to age, sex, and BMI matched non-CAD controls. Plasma WNT5A was positively and independently associated with both coronary calcification progression and new onset calcification in humans, suggesting that it has a clinically relevant role in vascular disease progression.

Previous reports have suggested that WNT5A may be involved in endothelial dysfunction, particularly in the context of diabetes (*22, 23*). These studies elegantly supported the notion that WNT5A signaling has vascular implications; however, the ability of WNT5A to regulate vascular redox state was unclear. Considering that obese individuals have elevated vascular oxidative stress due to activation of NADPH oxidases, we hypothesised that AT-derived WNT5A is a link between dysfunctional AT and vascular disease in obesity, and this could be mediated by its effects on human arterial redox state. Redox signaling is directly involved in multiple vascular diseases commonly presented as complications of obesity (*24-26*). NADPH oxidases comprise major sources of ROS in the human vascular wall (*8*). The activation of NOX1 and NOX2 isoforms of NADPH oxidases is dependent on the activation and membrane translocation of RAC1and P47$_{phox}$ cytoplasmic subunits in order to form the active enzymatic complex (*27*). Given that non-canonical Wnt signaling has been linked with activation of small GTPases like Rac, we hypothesised that adipose tissue-derived WNT5A may drive arterial oxidative stress via RAC1-mediated NADPH oxidases activation in obesity, as well as by eNOS uncoupling via BH4 oxidation.

Here we demonstrated that high WNT5A/SFRP5 ratio, either in plasma or in PVAT surrounding human arteries, is related to significantly higher $O_{2}.-$ generation in these vessels. The causal association of WNT5A with human arterial $O_{2}.-$ was subsequently confirmed using *ex vivo* models of human arteries, and the precise mechanisms were further elucidated *in vitro* using primary human VSMCs. The *in vivo* effects of WNT5A on vascular NADPH oxidases activity was then confirmed using a doxycycline-inducible tet-O- WNT5A model. WNT5A

appears to trigger non-canonical Wnt signaling at low (physiological) concentrations, as confirmed in our work, whereas high, supra-physiological concentrations of WNT5A may trigger canonical Wnt signaling. The effect of physiological concentrations of WNT5A on cellular redox state in human VSMCs is mediated by Fzd2 receptor-induced non-canonical activation of RAC1, resulting in the translocation of GTP- RAC1 and $P47_{phox}$ to the cell membrane and leading to enzymatic stimulation of NADPH oxidases in the vasculature. Co-culture of human adipocytes with human VSMCs revealed that knocking-down WNT5A in human pre-adipocytes results into a reduction of $O_{2.-}$ generation by NOX2in VSMCs, confirming the paracrine role of adipocyte-derived WNT5A on vascular redox state.

The balance between VSMCs migration and proliferation versus apoptosis is crucial for the stability of atherosclerotic plaques (*28*). Migration of these cells is believed to contribute to atherogenesis, particularly at the early disease stage (*29*). VSMCs may undergo a phenotypic switch whereby they lose their contractile phenotype markers and start producing metalloproteinases which may lead to fibrous cap thinning a plaque rupture (*28*). Previous studies have linked WNT5A signaling to reduced VSMCs apoptosis (*30*), but this effect was attributed to canonical Wnt signaling achieved using a supra-physiological WNT5A concentration in vitro (*30*). Conversely, WNT5A stimulates cellular motility and migration via non-canonical signaling in a variety of cell types (*31, 32*), while oxidative stress can also promote the migration of VSMCs (*9*). In this context, we hypothesised that WNT5A may affect VSMC phenotype and specifically lead to VSMC migration at least partially via induction of redox signaling.

We demonstrated that WNT5A induces migration of human VSMCs in a redox-sensitive manner which is reversed by peg-SOD, a scavenger of intracellular $O_{2.-}$. WNT5A may cause a VSMC phenotypic switch, evidenced by downregulation of contractile gene markers *ACTA2* and *TAGLN* (*28*) and a concomitant increase in the bioavailability of MMP9, a

metalloproteinase with strong associations with plaque rupture (*33*). Transcriptome analysis revealed that WNT5A regulates a number of migration-related genes in human VSMCs, thus potentially exerting multiple effects on VSMC migration. USP17, a deubiquitinating enzyme acting as a known activator of small GTPases like RAC (*18*), was the top hit up-regulated by WNT5A (and partly reversed by peg-SOD) in VSMCs. The USP17/ RAC1 link has previously been implicated in diseases in which cell motility plays a pivotal role, such as tumorigenesis (*34*). However, USP17 has not previously been implicated in vascular biology, nor has it been proposed as a downstream target of WNT5A signaling. Our data supports a role for USP17 in mediating the effects of WNT5A on RAC1activation and controlling vascular redox state, while the link between WNT5A and USP17 also appears to be partly redox-sensitive. These data identify the WNT5A/USP17/RAC1/NADPH oxidases axis as a potential therapeutic target to modify the vascular effects of obesity.

A limitation of the current study is the lack of *in vivo* mechanistic data linking WNT5A overexpression with atherosclerosis. Although we demonstrated that high plasma concentrations of WNT5A were related to faster progression of coronary atherosclerosis and development of new coronary calcified plaques in humans, an *in vivo* experimental model would potentially prove causality of this association. Further, prospectively designed, clinical studies are required to determine the prognostic value of circulating WNT5A as a biomarker for the prediction of vascular disease related outcomes (e.g., calcified plaque progression, clinical endpoints such as non-fatal myocardial infarction, stroke, cardiac mortality). Finally it remains unclear whether WNT5A secretion from the adipose tissue and/or WNT5A-reated vascular signalling could be targeted therapeutically, and whether such an intervention would have the potential to prevent the vascular complications of obesity.

Obesity is associated with enhanced activation of non-canonical Wnt signaling in the human arterial wall resulting from a shift in the balance between WNT5A and SFRP5 both in the

circulation and in PVAT and up-regulation of the WNT5A receptors Fzd2 and 5 on the arterial wall. This results in USP17-mediated activation of RAC1 and downstream activation of vascular NADPH oxidases, leading to $O_2^{.-}$ -induced migration of VSMCs. At a clinical level, WNT5A concentration is independently associated with the presence of CAD and progression of calcified coronary atherosclerotic plaque burden. These data identify UPS17 and WNT5A as rational targets for the prevention and /or treatment of vascular complications associated with obesity in humans.

Methods

Study design

The aim of this work was to explore the role of AT-derived WNT5A in regulating vascular redox signalling and vascular disease progression in humans. We hypothesised that WNT5A would be upregulated in obesity and would be able to induce vascular NADPH oxidase activation via RAC1 signalling, which could have downstream redox signalling effects triggering vascular disease.

To address these hypotheses, we first explored the associations between obesity, arterial $O_2^{.-}$ generation and the bioavailability of WNT5A in the circulation and a variety of AT depots (ScAT, ThAT, PVAT) in a cohort of 1,004 patients undergoing cardiac surgery (study 1, see below). These were used to provide observational insights as to the relationship of WNT5A with arterial oxidative stress in the context of obesity. Power size calculations for these clinical studies indicated that we would need 933 patients to detect a 10% difference in arterial NADPH-stimulated $O_2^{.-}$ between the low and high plasma WNT5A/SFRP5 tertile with $\alpha = 0.05$ and power of 0.90 assuming an SD of 100 RLU/sec/mg tissue.

The clinical link of circulating WNT5A with parameters of vascular disease (presence of CAD, calcified plaque progression, new onset calcification) was tested in a validation study of 70 CAD patients matched with 70 non-CAD controls (study 2, see below) and a follow-up study of CCS monitoring in patients having undergone two cardiac CT scans, where baseline and follow-up CCS scores were evaluated and circulating WNT5A was quantified. With 70 patients per group, we could detect a difference of 10ng/mL in plasma WNT5A with $\alpha = 0.05$ and power 0.9 (assuming plasma WNT5A SD = 9ng/mL).

Ex vivo mechanistic experiments were employed to test the direct signalling effects of WNT5A incubations on human arteries harvested during surgery, in a series of mechanistic experiments performed in a paired design for individuals patients. Based on previous work from our group, we estimated that with a minimum of 5 pairs of samples (serial rings from the same vessel) we would be able to identify a change of $\log(O_{2.-})$ by 0.48 with $\alpha = 0.05$, power 0.9 and SD for a difference in the response of the pairs of 0.25.

The effect of WNT5A on arterial $O_{2.-}$ production was validated with a short-term proof-of-concept mouse experiment of global inducible *Wnt5a* overexpression upon doxycycline treatment. We estimated that with 5 mice per group we could detect a difference of 250 RLU/sec/mg tissue in aortic $O_{2.-}$ with $\alpha = 0.05$ and power 0.9 assuming an aortic NADPH-stimulated $O_{2.-}$ SD of 120 RLU/sec/mg tissue).

The integrated effects of WNT5A on vascular redox state and downstream redox signalling events such as cell migration were evaluated in vitro in primary VSMCs isolated from human vascular segments. Similarly to the ex vivo experiments, we estimated that with 5 pairs of wells we would be able to identify a change of 175 RLU/sec/μg protein in VSMC NADPH-stimulated $O_{2.-}$ with $\alpha=0.05$, power 0.9 and SD = 85 RLU/sec/μg protein.

Human study protocols were in agreement with the Declaration of Helsinki and all patients provided written informed consent prior to enrolment. All studies (clinical or experimental) were performed blinded. Human studies were approved by local research ethics committees (under RECs 11/SC/0140 and 15/SC/0545). All animal studies were conducted with ethical approval from the Local Ethical Review Committee and in accordance with the UK Home Office regulations (Guidance on the Operation of Animals, Scientific Procedures Act, 1986).

Human studies protocols

Study protocols were in agreement with the Declaration of Helsinki and all patients provided written informed consent prior to enrolment. The demographic characteristics of the participants of all study arms are presented in table S1. Hyperlipidaemia and hypertension were defined according to the latest European Society Cardiology Guidelines (*35, 36*). Diabetes mellitus was defined according to the American Diabetes Association guidelines (*37*). Obesity was defined according to the Adult Treatment Panel (ATP) III guidelines (*38*).

In vivo clinical studies (studies 1-3)

Study 1 comprised 1,004 prospectively enrolled patients undergoing cardiac surgery [including coronary artery bypass grafting (CABG) and valve replacement/repair] at the John Radcliffe hospital, Oxford University NHS Foundation Trust, UK. Exclusion criteria included inflammatory, neoplastic, renal, or hepatic diseases. Fasting blood samples were obtained on the morning of surgery and were used for plasma isolation for circulating biomarker measurements. During surgery, segments of the IMA with its surrounding PVAT, ThAT from the paracardial region, and ScAT from the chest were collected, transferred to the lab on ice,

and processed for ex vivo experiments, vasomotor studies, and measurement of vascular O_{2}^{-}.

Study 2 included 70 individuals with CAD and 70 controls without CAD (confirmed with coronary CT angiography). Individuals were matched for age, gender, and BMI for cross-sectional studies comparing circulating WNT5A and SFRP5. Study 3 consisted of 68 individuals that underwent two non-contrast CT scans 3-5 years apart (48.5 ± 5.8 months), to study progression of atherosclerotic disease in the coronary arteries. The development of new calcification and the progression of existing calcified atherosclerotic plaques were compared between the two scans.

Ex vivo studies with human vessels (study 4)

The human ex vivo study (study 4) included 94 patients undergoing cardiac surgery at the John Radcliffe hospital, Oxford University NHS Foundation Trust, UK. Patients were prospectively recruited and patients with inflammatory, neoplastic, renal or hepatic diseases were excluded. Human IMA and saphenous vein (SV) segments were collected during surgery and transferred to the lab on ice. IMA samples were processed in the lab as explained in relevant sections, subjected to *ex vivo* incubations and ultimately used for vascular O_{2}^{-} quantification, vasomotor studies, biopterin measurements and downstream signaling evaluation as described later.

In vivo animal studies

A doxycycline-inducible WNT5A knock-in mouse model was used to determine the *in vivo* effects of WNT5A on vascular NADPH oxidases activity. FVB/N Tg(tetO- *Wnt5a*)17Rva/J mice were obtained from Jackson Laboratories (stock #022938), and crossed to mixed background C57BL/6, 129/SV, FVB CAGG-*rtTA* (generated by Dr Lukas Dow in the lab of

Dr Scott Lowe at Memorial Sloan Kettering Cancer Centre, USA) (*39*). Mice were backcrossed to C57BL/6 background seven times prior to the study. TetO-W*nt5a+* and *rtTA+* mice were then crossed obtaining double transgenic mice, *rtTA+* single transgenic mice were kept as control animals. 2mg/mL doxycycline hyclate (J60579, Alfa Aesar) was administered, to both double transgenic tetO- *Wnt5a+*/*rtTA+* and control tetO-*Wnt5a–*/rtTA+ animals via the drinking water, containing 5% sucrose overnight to induce *Wnt5a* expression. Considerable weight loss (up to ~15% of body weight) was observed after three days of doxycycline treatment, therefore this mouse model was not suitable for long-term experiments as per local committee ethics. Overnight doxycycline treatment induced minor weight loss and did not compromise the welfare of the animals. DNA extracted from experimental animal ear notches was used for genotyping with the following PCR primers:

C57BL/6, FVB CAG-*rtTA*

  CCM   5'- CGAAACTCTGGTTGACATG - 3'

  CTG   5'- ATGCCCTGGCTCACAAATAC - 3'

  CWT   5'- TGCCTATCATGTTGTCAAA – 3'

C57BL/6, FVB/N Tg(tetO- *Wnt5a*)17Rva/J

  17815   5'- ACAAAGACGATGACGACAAGC – 3'

  17816   5'- CGCACCTTCTCCAATGTACTG – 3'

  oIMR7338   5'- CTAGGCCACAGAATTGAAAGATCT – 3'

  oIMR7339   5' – GTAGGTGGAAATTCTAGCATCATCC – 3'

Mice were housed in a specific pathogen-free environment, in Tecniplast Sealsafe IVC cages (floor area 542 cm2) with a maximum of six other mice. Mice were kept in a 12 h light/dark

cycle and in controlled temperatures (20–22°C) and fed normal chow and water ad libitum. A detailed phenotyping of the mouse model is presented in fig. S4.

Blood Sampling and Circulating Biomarker Measurements

Humans

Preoperative venous blood samples were collected from subjects of Study 1 after 8h of fasting and in particular on the morning of surgery as previously described (*40*). Blood samples were also collected from subjects of Study 2 after 8h of fasting upon admission. Similarly, blood samples from Study 3 participants were collected after 8h of fasting just prior to the cardiac CT scans. After centrifugation at 2000 g at 4°C for 15 min, plasma was collected and stored at −80 °C until assayed. Plasma WNT5A and SFRP5 were measured by using commercially available ELISA kits (Cloud Clone Corp, catalogue number SEP549Hu and MyBiosource, catalogue number MBS702373 respectively) following the manufacturer's instructions.

Mice

900 µl blood was drawn from the vena cava into a syringe containing sodium heparin. Blood samples were centrifuged for 15 minutes at 3,000 rpm at room temperature. Plasma was subsequently centrifuged for 5 minutes at 13,000 rpm to remove remaining cells and platelets and immediately frozen at -80°C. Plasma WNT5A was measured by using a commercially available ELISA kit (Cloud Clone Corp, catalogue number SEP549Mu) following the manufacturer's instructions.

Human Adipose Tissue and Vessel Harvesting

Internal mammary artery (IMA) samples were harvested with a "no touch" technique with their perivascular tissue (PVAT) at the time of CABG as we have described previously (*42*). Vascular segments were transferred into oxygenated (95% O_2/5% CO_2) ice-cold Krebs Hensleit buffer and the vessel lumen was flushed gently by using an insulin syringe to remove blood. Each vessel was separated from its surrounding adipose tissue in the lab, under magnification by the same operator, to limit the between-patients variability. The same anaesthetics were used in all cases, and each sample was always obtained at the same stage of the operation, to limit inter-patient variability. ThAT and ScAT specimens were collected during surgery, then snap-frozen in TRI reagent (Sigma, catalogue number T9424) and stored at -80$_o$C until used for RNA isolation.

Transcriptome Profiling of WNT5A-Treated VSMCs

Treatments and RNA Extraction

VSMCs isolated from five individual patients were incubated 8 hours with 100 ng/mL WNT5A or 100 U/mL peg-SOD. Patients were selected to be obese and without diabetes mellitus, allowing us to evaluate the integrated effects of WNT5A in the clinically relevant setting of obesity. RNA was extracted from VSMCs using the MagMAX mirVana total RNA isolation kit (Thermo Fischer Scientific, Catalogue Number A27828) as mentioned earlier, and processed for high throughput gene expression profiling.

GeneChip Human Transcriptome Array 2.1

The genome-wide expression profiling was carried out at the High Throughput Genomics Wellcome Trust Centre for Human Genetics (Oxford, UK). RNA samples were processed

using the Affymetrix GeneChip WT PLUS Reagent kit, the manual target preparation for GeneChip whole transcript expression arrays. The labelled ss-cDNA were then hybridised to the Affymetrix HuGene-2.1-st Array Plate and processed on the Affymetrix GeneTitan platform. The microarray data generated by this study have been submitted to GEO depository under ID GSE109859.

Statistical analysis

Continuous variables were tested for normal distribution using the Kolmogorov-Smirnov test. Non-normally distributed variables are presented as median[25th-75th percentile] and whiskers (Tukey). Normally distributed variables are presented as mean±SEM. Comparisons of continuous variables between two groups were performed using unpaired t test or Man-Whitney U-test as appropriate, while comparisons between 3 or more groups were performed using one-way ANOVA or Kruskal-Wallis followed by Bonferroni or Dunn's post hoc correction for multiple comparisons. Paired comparisons were performed using paired t test or Wilcoxon signed-rank test as appropriate. For between-groups serial changes we used two-way ANOVA for repeated measures with interaction terms as presented in the figure legends.

To examine whether the association between obesity and vascular NADPH oxidase activity is independent of *WNT5A*/*SFRP5* expression in PVAT, we performed multivariate linear regression where NADPH-stimulated O_{2^-} was used as dependent variable and obesity classification, age, sex, diabetes, hypertension and smoking (with/without the addition of *WNT5A*/*SFRP5* expression tertiles in PVAT) were used as independent variables. The relevant standardised beta coefficients are presented. To address whether plasma WNT5A, SFRP5 and the ratio of the two were independently associated with the presence of CAD in the nested case-control study 2, we performed multivariate linear egression in which the presence of CAD was

used as dependent variable and hypertension, hyperlipidaemia, smoking and plasma WNT5A or SFRP5or WNT5A/SFRP5 ratio were used as independent variables. The standardized beta (Bstand) is presented for each variable. To examine whether coronary calcified plaque progression or new onset calcification were associated with plasma WNT5A, we performed multivariate linear regression where calcified plaque progression and new onset calcification were used as dependent variables and plasma WNT5A, age and sex were used as independent variables. All statistical tests were two-tailed and were performed using SPSS version 20.0. *P<0.05* was considered statistically significant.

With regards to microarray data processing, normalisation, quality control and differential gene expression analysis was performed with the Affymetrix Transcriptome Analysis Console (TAC 4.0) Software. The statistical comparisons between treatments was done following a repeated measures model for the individual patients.WNT5A pathway enrichment analysis was carried out in ConsensusPathDB-human with differentially expressed genes (DEGs) (WNT5A -treated vs. untreated-controls) that displayed fold change (linear)>1 or <-1 and a p-value (condition pair)< 0.05. Gene Ontology database was used to functionally annotate DEGs.

Supplementary material list

Materials and methods

Fig. S1. *WNT5A & SFRP5* expression data in subcutaneous adipose tissue (ScAT), internal mammary arteries (IMAs) and perivascular adipose tissue (PVAT)

Fig. S2: Ex vivo effect of WNT5A on NOX isoform gene expression in internal mammary arteries (IMAs)

Fig. S3: Association of plasma WNT5A/SFRP5 with arterial *NOX* expression

Fig. S4: Effects of WNT5A on endothelial function and endothelial nitric oxide synthase (eNOS) coupling

Fig. S5. Phenotyping of the TetO-*Wnt5a* rtTA mouse model

Fig. S6: Phenotyping of isolated primary vascular smooth muscle cells (VSMCs)

Fig. S7: WNT5A dysregulated genes and pathways and effects on vascular smooth muscle cell (VSMC) migration

Fig. S8: WNT5A and vascular smooth muscle cell (VSMC) phenotypic switch

Fig. S9: Ubiquitin-specific protease 17 (USP17) as the maximally upregulated target in response to WNT5A and USP17 transfection in HeLa cells

Fig. S10: Schematic diagram with proposed mechanism

Table S1. Demographic characteristics of the study participants

Table S2. Demographic characteristics of study 1 participants per body mass index (BMI) group

Table S3. Multivariate linear regression models of calcified plaque progression and new-onset calcification

Table S4. Multivariate linear regression models of arterial NADPH-stimulated superoxide ($O_2 \cdot^-$) production

References

1.   M. Bastien, P. Poirier, I. Lemieux, J. P. Despres, Overview of epidemiology and contribution of obesity to cardiovascular disease. *Prog Cardiovasc Dis* **56**, 369-381 (2014).

2.   D. Aune, A. Sen, M. Prasad, T. Norat, I. Janszky, S. Tonstad, P. Romundstad, L. J. Vatten, BMI and all cause mortality: systematic review and non-linear dose-response meta-analysis of 230 cohort studies with 3.74 million deaths among 30.3 million participants. *BMJ* **353**, i2156 (2016).

3.   P. Arner, J. Backdahl, P. Hemmingsson, P. Stenvinkel, D. Eriksson-Hogling, E. Naslund, A. Thorell, D. P. Andersson, K. Caidahl, M. Ryden, Regional variations in the relationship between arterial stiffness and adipocyte volume or number in obese subjects. *Int J Obes (Lond)* **39**, 222-227 (2015).

4.   I. Akoumianakis, A. Tarun, C. Antoniades, Perivascular adipose tissue as a regulator of vascular disease pathogenesis: identifying novel therapeutic targets. *Br J Pharmacol* **174**, 3411-3424 (2017).

5.   J. J. Fuster, N. Ouchi, N. Gokce, K. Walsh, Obesity-Induced Changes in Adipose Tissue Microenvironment and Their Impact on Cardiovascular Disease. *Circ Res* **118**, 1786-1807 (2016).

6.   E. K. Oikonomou, C. Antoniades, Immunometabolic Regulation of Vascular Redox State: The Role of Adipose Tissue. *Antioxid Redox Signal*, (2017).

7.   H. Li, S. Horke, U. Forstermann, Vascular oxidative stress, nitric oxide and atherosclerosis. *Atherosclerosis* **237**, 208-219 (2014).

8.   A. Konior, A. Schramm, M. Czesnikiewicz-Guzik, T. J. Guzik, NADPH oxidases in vascular pathology. *Antioxid Redox Signal* **20**, 2794-2814 (2014).

9.   C. A. Papaharalambus, K. K. Griendling, Basic mechanisms of oxidative stress and reactive oxygen species in cardiovascular injury. *Trends Cardiovasc Med* **17**, 48-54 (2007).

10.   A. Kikuchi, H. Yamamoto, A. Sato, Selective activation mechanisms of Wnt signaling pathways. *Trends Cell Biol* **19**, 119-129 (2009).

11.   Y. Kawano, R. Kypta, Secreted antagonists of the Wnt signaling pathway. *J Cell Sci* **116**, 2627-2634 (2003).

12.   M. T. Veeman, J. D. Axelrod, R. T. Moon, A second canon. Functions and mechanisms of beta-catenin-independent Wnt signaling. *Dev Cell* **5**, 367-377 (2003).

13.   M. Reis, S. Liebner, Wnt signaling in the vasculature. *Exp Cell Res* **319**, 1317-1323 (2013).

14. N. Ouchi, A. Higuchi, K. Ohashi, Y. Oshima, N. Gokce, R. Shibata, Y. Akasaki, A. Shimono, K. Walsh, SFRP5 is an anti-inflammatory adipokine that modulates metabolic dysfunction in obesity. *Science* **329**, 454-457 (2010).

15. I. Ackers, C. Szymanski, K. J. Duckett, L. A. Consitt, M. J. Silver, R. Malgor, Blocking WNT5A signaling decreases CD36 expression and foam cell formation in atherosclerosis. *Cardiovasc Pathol* **34**, 1-8 (2018).

16. D. M. Schulte, N. Muller, K. Neumann, F. Oberhauser, M. Faust, H. Gudelhofer, B. Brandt, W. Krone, M. Laudes, Pro-inflammatory WNT5A and anti-inflammatory SFRP5 are differentially regulated by nutritional factors in obese human subjects. *PLoS One* **7**, e32437 (2012).

17. J. F. Burrows, M. J. McGrattan, J. A. Johnston, The DUB/USP17 deubiquitinating enzymes, a multigene family within a tandemly repeated sequence. *Genomics* **85**, 524-529 (2005).

18. M. de la Vega, A. A. Kelvin, D. J. Dunican, C. McFarlane, J. F. Burrows, J. Jaworski, N. J. Stevenson, K. Dib, J. Z. Rappoport, C. J. Scott, A. Long, J. A. Johnston, The deubiquitinating enzyme USP17 is essential for GTPase subcellular localization and cell motility. *Nat Commun* **2**, 259 (2011).

19. I. Akoumianakis, C. Antoniades, The interplay between adipose tissue and the cardiovascular system: is fat always bad? *Cardiovasc Res* **113**, 999-1008 (2017).

20. N. Alexopoulos, D. Katritsis, P. Raggi, Visceral adipose tissue as a source of inflammation and promoter of atherosclerosis. *Atherosclerosis* **233**, 104-112 (2014).

21. V. Catalan, J. Gomez-Ambrosi, A. Rodriguez, A. I. Perez-Hernandez, J. Gurbindo, B. Ramirez, L. Mendez-Gimenez, F. Rotellar, V. Valenti, R. Moncada, P. Marti, I. Sola, C. Silva, J. Salvador, G. Fruhbeck, Activation of noncanonical Wnt signaling through WNT5A in visceral adipose tissue of obese subjects is related to inflammation. *J Clin Endocrinol Metab* **99**, E1407-1417 (2014).

22. M. G. Farb, S. Karki, S. Y. Park, S. M. Saggese, B. Carmine, D. T. Hess, C. Apovian, J. L. Fetterman, R. Breton-Romero, N. M. Hamburg, J. J. Fuster, M. A. Zuriaga, K. Walsh, N. Gokce, WNT5A-JNK regulation of vascular insulin resistance in human obesity. *Vasc Med* **21**, 489-496 (2016).

23. R. Breton-Romero, B. Feng, M. Holbrook, M. G. Farb, J. L. Fetterman, E. A. Linder, B. D. Berk, N. Masaki, R. M. Weisbrod, E. Inagaki, N. Gokce, J. J. Fuster, K. Walsh, N. M. Hamburg, Endothelial Dysfunction in Human Diabetes Is Mediated by WNT5A-JNK Signaling. *Arterioscler Thromb Vasc Biol* **36**, 561-569 (2016).

24. J. F. Keaney, Jr., M. G. Larson, R. S. Vasan, P. W. Wilson, I. Lipinska, D. Corey, J. M. Massaro, P. Sutherland, J. A. Vita, E. J. Benjamin, S. Framingham, Obesity and systemic oxidative stress: clinical correlates of oxidative stress in the Framingham Study. *Arterioscler Thromb Vasc Biol* **23**, 434-439 (2003).

25. A. Ceriello, E. Motz, Is oxidative stress the pathogenic mechanism underlying insulin resistance, diabetes, and cardiovascular disease? The common soil hypothesis revisited. *Arterioscler Thromb Vasc Biol* **24**, 816-823 (2004).

26. I. Akoumianakis, C. Antoniades, Impaired Vascular Redox Signaling in the Vascular Complications of Obesity and Diabetes Mellitus. *Antioxid Redox Signal*, (2018).

27. T. J. Guzik, D. G. Harrison, Vascular NADPH oxidases as drug targets for novel antioxidant strategies. *Drug Discov Today* **11**, 524-533 (2006).

28. M. R. Bennett, S. Sinha, G. K. Owens, Vascular Smooth Muscle Cells in Atherosclerosis. *Circ Res* **118**, 692-702 (2016).

29. J. Chappell, J. L. Harman, V. M. Narasimhan, H. Yu, K. Foote, B. D. Simons, M. R. Bennett, H. F. Jorgensen, Extensive Proliferation of a Subset of Differentiated, yet

Plastic, Medial Vascular Smooth Muscle Cells Contributes to Neointimal Formation in Mouse Injury and Atherosclerosis Models. *Circ Res* **119**, 1313-1323 (2016).

30. C. Mill, B. A. Monk, H. Williams, S. J. Simmonds, J. Y. Jeremy, J. L. Johnson, S. J. George, WNT5A-induced Wnt1-inducible secreted protein-1 suppresses vascular smooth muscle cell apoptosis induced by oxidative stress. *Arterioscler Thromb Vasc Biol* **34**, 2449-2456 (2014).

31. M. K. Hasan, J. Yu, L. Chen, B. Cui, G. F. Widhopf Ii, L. Rassenti, Z. Shen, S. P. Briggs, T. J. Kipps, WNT5A induces ROR1 to complex with HS1 to enhance migration of chronic lymphocytic leukemia cells. *Leukemia* **31**, 2615-2622 (2017).

32. A. Kikuchi, H. Yamamoto, A. Sato, S. Matsumoto, WNT5A: its signaling, functions and implication in diseases. *Acta Physiol (Oxf)* **204**, 17-33 (2012).

33. A. Yabluchanskiy, Y. Ma, R. P. Iyer, M. E. Hall, M. L. Lindsey, Matrix metalloproteinase-9: Many shades of function in cardiovascular disease. *Physiology (Bethesda)* **28**, 391-403 (2013).

34. C. McFarlane, A. A. Kelvin, M. de la Vega, U. Govender, C. J. Scott, J. F. Burrows, J. A. Johnston, The deubiquitinating enzyme USP17 is highly expressed in tumor biopsies, is cell cycle regulated, and is required for G1-S progression. *Cancer Res* **70**, 3329-3339 (2010).

35. A. L. Catapano, I. Graham, G. De Backer, O. Wiklund, M. J. Chapman, H. Drexel, A. W. Hoes, C. S. Jennings, U. Landmesser, T. R. Pedersen, Z. Reiner, G. Riccardi, M. R. Taskinen, L. Tokgozoglu, W. M. M. Verschuren, C. Vlachopoulos, D. A. Wood, J. L. Zamorano, M. T. Cooney, E. S. C. S. D. Group, 2016 ESC/EAS Guidelines for the Management of Dyslipidaemias. Eur Heart J 37, 2999-3058 (2016).

36. G. Mancia, R. Fagard, K. Narkiewicz, J. Redon, A. Zanchetti, M. Bohm, T. Christiaens, R. Cifkova, G. De Backer, A. Dominiczak, M. Galderisi, D. E. Grobbee, T. Jaarsma, P. Kirchhof, S. E. Kjeldsen, S. Laurent, A. J. Manolis, P. M. Nilsson, L. M. Ruilope, R. E. Schmieder, P. A. Sirnes, P. Sleight, M. Viigimaa, B. Waeber, F. Zannad, J. Redon, A. Dominiczak, K. Narkiewicz, P. M. Nilsson, M. Burnier, M. Viigimaa, E. Ambrosioni, M. Caufield, A. Coca, M. H. Olsen, R. E. Schmieder, C. Tsioufis, P. van de Borne, J. L. Zamorano, S. Achenbach, H. Baumgartner, J. J. Bax, H. Bueno, V. Dean, C. Deaton, C. Erol, R. Fagard, R. Ferrari, D. Hasdai, A. W. Hoes, P. Kirchhof, J. Knuuti, P. Kolh, P. Lancellotti, A. Linhart, P. Nihoyannopoulos, M. F. Piepoli, P. Ponikowski, P. A. Sirnes, J. L. Tamargo, M. Tendera, A. Torbicki, W. Wijns, S. Windecker, D. L. Clement, A. Coca, T. C. Gillebert, M. Tendera, E. A. Rosei, E. Ambrosioni, S. D. Anker, J. Bauersachs, J. B. Hitij, M. Caulfield, M. De Buyzere, S. De Geest, G. A. Derumeaux, S. Erdine, C. Farsang, C. Funck-Brentano, V. Gerc, G. Germano, S. Gielen, H. Haller, A. W. Hoes, J. Jordan, T. Kahan, M. Komajda, D. Lovic, H. Mahrholdt, M. H. Olsen, J. Ostergren, G. Parati, J. Perk, J. Polonia, B. A. Popescu, Z. Reiner, L. Ryden, Y. Sirenko, A. Stanton, H. Struijker-Boudier, C. Tsioufis, P. van de Borne, C. Vlachopoulos, M. Volpe, D. A. Wood, 2013 ESH/ESC guidelines for the management of arterial hypertension: the Task Force for the Management of Arterial Hypertension of the European Society of Hypertension (ESH) and of the European Society of Cardiology (ESC). Eur Heart J 34, 2159-2219 (2013).

37. L. Garza, J. Dols, M. Gillespie, An initiative to improve primary prevention of cardiovascular disease in adults with type II diabetes based on the ACC/AHA (2013) and ADA (2016) guidelines. J Am Assoc Nurse Pract 29, 606-611 (2017).

38. E. National Cholesterol Education Program Expert Panel on Detection, A. Treatment of High Blood Cholesterol in, Third Report of the National Cholesterol Education Program (NCEP) Expert Panel on Detection, Evaluation, and Treatment of High

Blood Cholesterol in Adults (Adult Treatment Panel III) final report. Circulation 106, 3143-3421 (2002).

39. P. K. Premsrirut, L. E. Dow, S. Y. Kim, M. Camiolo, C. D. Malone, C. Miething, C. Scuoppo, J. Zuber, R. A. Dickins, S. C. Kogan, K. R. Shroyer, R. Sordella, G. J. Hannon, S. W. Lowe, A rapid and scalable system for studying gene function in mice using conditional RNA interference. *Cell* **145**, 145-158 (2011).

40. A. S. Antonopoulos, M. Margaritis, P. Coutinho, C. Shirodaria, C. Psarros, L. Herdman, F. Sanna, R. De Silva, M. Petrou, R. Sayeed, G. Krasopoulos, R. Lee, J. Digby, S. Reilly, C. Bakogiannis, D. Tousoulis, B. Kessler, B. Casadei, K. M. Channon, C. Antoniades, Adiponectin as a link between type 2 diabetes and vascular NADPH oxidase activity in the human arterial wall: the regulatory role of perivascular adipose tissue. *Diabetes* **64**, 2207-2219 (2015).

41. A. S. Agatston, W. R. Janowitz, F. J. Hildner, N. R. Zusmer, M. Viamonte, Jr., R. Detrano, Quantification of coronary artery calcium using ultrafast computed tomography. *J Am Coll Cardiol* **15**, 827-832 (1990).

42. C. Antoniades, C. Shirodaria, N. Warrick, S. Cai, J. de Bono, J. Lee, P. Leeson, S. Neubauer, C. Ratnatunga, R. Pillai, H. Refsum, K. M. Channon, 5-methyltetrahydrofolate rapidly improves endothelial function and decreases superoxide production in human vessels: effects on vascular tetrahydrobiopterin availability and endothelial nitric oxide synthase coupling. *Circulation* **114**, 1193-1201 (2006).

43. M. Margaritis, A. S. Antonopoulos, J. Digby, R. Lee, S. Reilly, P. Coutinho, C. Shirodaria, R. Sayeed, M. Petrou, R. De Silva, S. Jalilzadeh, M. Demosthenous, C. Bakogiannis, D. Tousoulis, C. Stefanadis, R. P. Choudhury, B. Casadei, K. M. Channon, C. Antoniades, Interactions between vascular wall and perivascular adipose tissue reveal novel roles for adiponectin in the regulation of endothelial nitric oxide synthase function in human vessels. *Circulation* **127**, 2209-2221 (2013).

44. C. Antoniades, C. Shirodaria, M. Crabtree, R. Rinze, N. Alp, C. Cunnington, J. Diesch, D. Tousoulis, C. Stefanadis, P. Leeson, C. Ratnatunga, R. Pillai, K. M. Channon, Altered plasma versus vascular biopterins in human atherosclerosis reveal relationships between endothelial nitric oxide synthase coupling, endothelial function and inflammation. *Circulation* **116**, 2851-2859 (2007).

45. C. Antoniades, C. Bakogiannis, P. Leeson, T. J. Guzik, M. H. Zhang, D. Tousoulis, A. S. Antonopoulos, M. Demosthenous, K. Marinou, A. Hale, A. Paschalis, C. Psarros, C. Triantafyllou, J. Bendall, B. Casadei, C. Stefanadis, K, M, Channon, Rapid, direct effects of statin treatment on arterial redox state and nitric oxide bioavailability in human atherosclerosis via tetrahydrobiopterin-mediated entohelial nitric oxide synthase coupling. *Circulation* **124**, 335-345 (2011).

46. M. W. Pfaffl, A new mathematical model for relative quantification in real-time RT-PCR. *Nucleic Acids Res* **29**, e45 (2001).

47. M. Todorcevic, C. Hilton, C. McNeil, C. Christodoulides, L. Hodson, F. Karpe, K. E. Pinnick, A cellular model for the investigation of depot specific human adipocyte biology. *Adipocyte* **6**, 40-55 (2017).

Author contributions: I.A. conceived and performed experiments, contributed to participant recruitment, performed data analysis and drafted the manuscript; F.S. conceived and performed experiments, performed data analysis and contributed to the writing of the manuscript; M.M. performed experiments, contributed to participant recruitment, performed data analysis and reviewed the manuscript; I.B. performed experiments and reviewed the manuscript; N.A. performed data analysis and reviewed the manuscript; LH. Contributed to participant recruitment, data collection and analysis; P.C. performed experiments; H.F. performed experiments; A.S.A. contributed to participant recruitment, performed experiments and data analysis and reviewed the manuscript; E.K.O. contributed to participant recruitment and reviewed the manuscript; S.T. contributed to participant recruitment and data collection; A.P.C performed experiments and reviewed the manuscript; S.C. performed experiments; C.P.K. performed experiments; C.C. provided experimental resources and expertise and reviewed the

manuscript; M.P. contributed to surgical specimen collection; G.K. contributed surgical specimen collection; R.S. contributed to surgical specimen collection; L.L. performed experiments; A.H. provided experimental resources and expertise; M.K. performed experiments; E.M. provided experimental resources and expertise; G.D. provided experimental resources and expertise; S.G. provided expertise and reviewed the manuscript; D.T. contributed to data analysis and reviewed the manuscript; K.M.C. contributed to the project design, provided experimental resources and expertise and reviewed the manuscript; C.A. conceived the project, secured funding, oversaw the implementation of individual experiments, performed data analysis and corrected the manuscript.
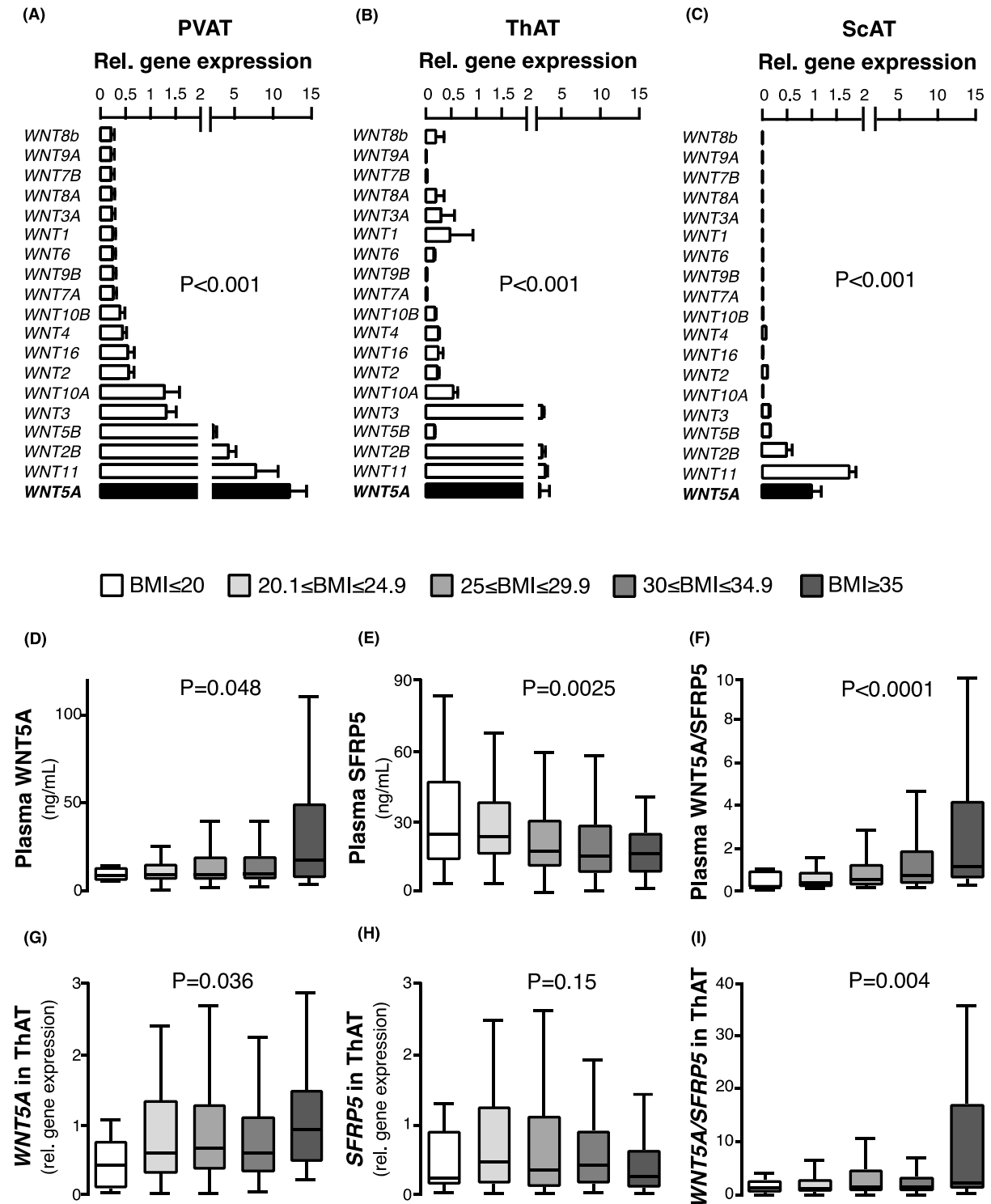
Fig. 1. Gene expression of Wnt ligands in adipose tissue and plasma concentration of

WNT5A/SFRP5 in obesity. (A-C) Gene expression of the 19 Wnt ligands in human (A)

perivascular (PVAT), (B) thoracic (ThAT), and (C) subcutaneous (ScAT) AT in $n = 54$ patients of study 1. (**D-F**) Circulating plasma concentrations of (D) WNT5A (range: 1 to 112 ng/ml), (E) decoy receptor SFRP5 , and (F) WNT5A/SFRP5 ratio in individuals of study 1. (**G-I**) Gene expression of (G) *WNT5A*, (B) *SFRP5*, and (C) the ratio of *WNT5A/SFRP5* in ThAT of study 1 participants. Study 1 participants per group: BMI: ≤20Kg/m2: 25; 20.1-24.9 Kg/m2: 217; 25-29.9 Kg/m2: 432; 30-34.9 Kg/m2: 233; ≥35 Kg/m2: 57. Data are presented as mean ± SEM (A-C) or median[25th-75th percentile] (D-I). *P* values in (A-C) are calculated by Friedman tests; *P* values in (D-I) are calculated by Kruskal Wallis tests. AT: adipose tissue; SEM: Standard error of the mean.
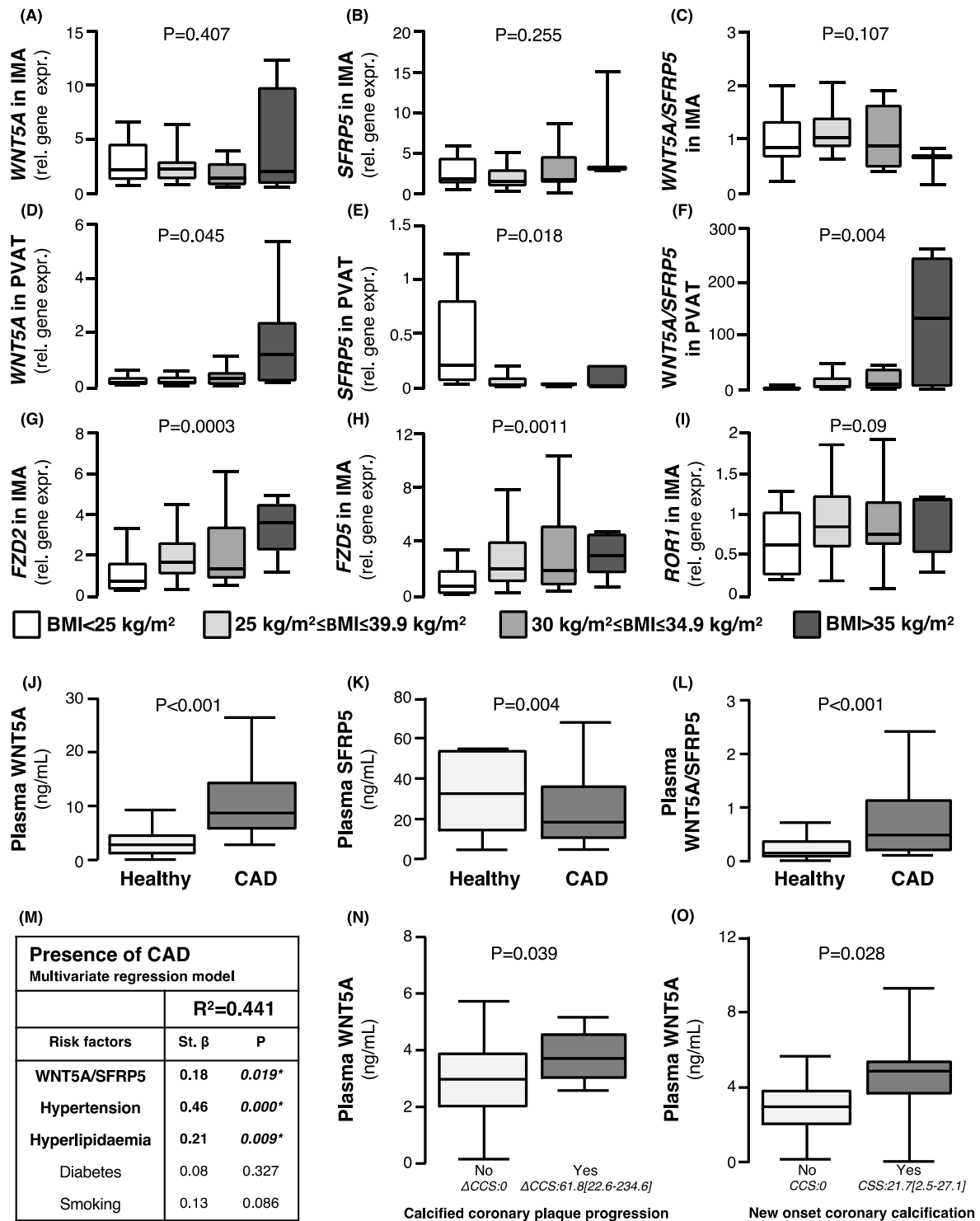
Fig. 2. Interactions between obesity, WNT5A/SFRP5, and vascular disease. (**A**-**C**) Gene expression of (A) *WNT5A,* (B) *SFRP5*, and (C) the ratio of *WNT5A/SFRP5* in IMAs according to BMI. (**D**-**F**) Gene expression of (D) *WNT5A,* (E) *SFRP5*, and (C) the ratio of *WNT5A/SFRP5* in PVAT according to BMI. (**G**-**I**) Gene expression of Wnt receptors (G) *FZD2,* (H) *FZD5,*

and (I) *ROR1* in IMAs according to BMI . (**J-L**) Circulating plasma concentrations of (J) WNT5A, (K) SFRP5, and (L) WNT5A/SFRP5 ratio in patients with CAD and healthy controls (*n* = 70). (**M**) Table of multivariable regression analysis of the association of circulating WNT5A, SFRP5, WNT5A/SFRP5, cardiovascular risk factors, and the presence of CAD in study 2 (*n* = 70). (**N**) Plasma WNT5A concentration in patients with or without coronary calcium score (CCS) progression (ΔCCS$\geq$1HU, 61.8[22.6-234.6], *n* = 68, study 3). (**O**) Plasma WNT5A concentration in patients with or without new onset calcification (follow-up CSS:21.7[2.5-27.1], n=38). (N-O) presented as median[25th-75th percentile]. Data are presented as median[25th-75th percentile]. *P* values in (A-N) are calculated by Kruskal Wallis tests. Study 1 participants with IMA/PVAT samples available for panels A-I were: BMI<25Kg/m2: 33; 25-29.9Kg/m2: 77; 30-30Kg/m2:42; >35 Kg/m2:13. IMA: internal mammary artery; BMI: body mass index; PVAT: perivascular adipose tissue; CAD: coronary artery disease.
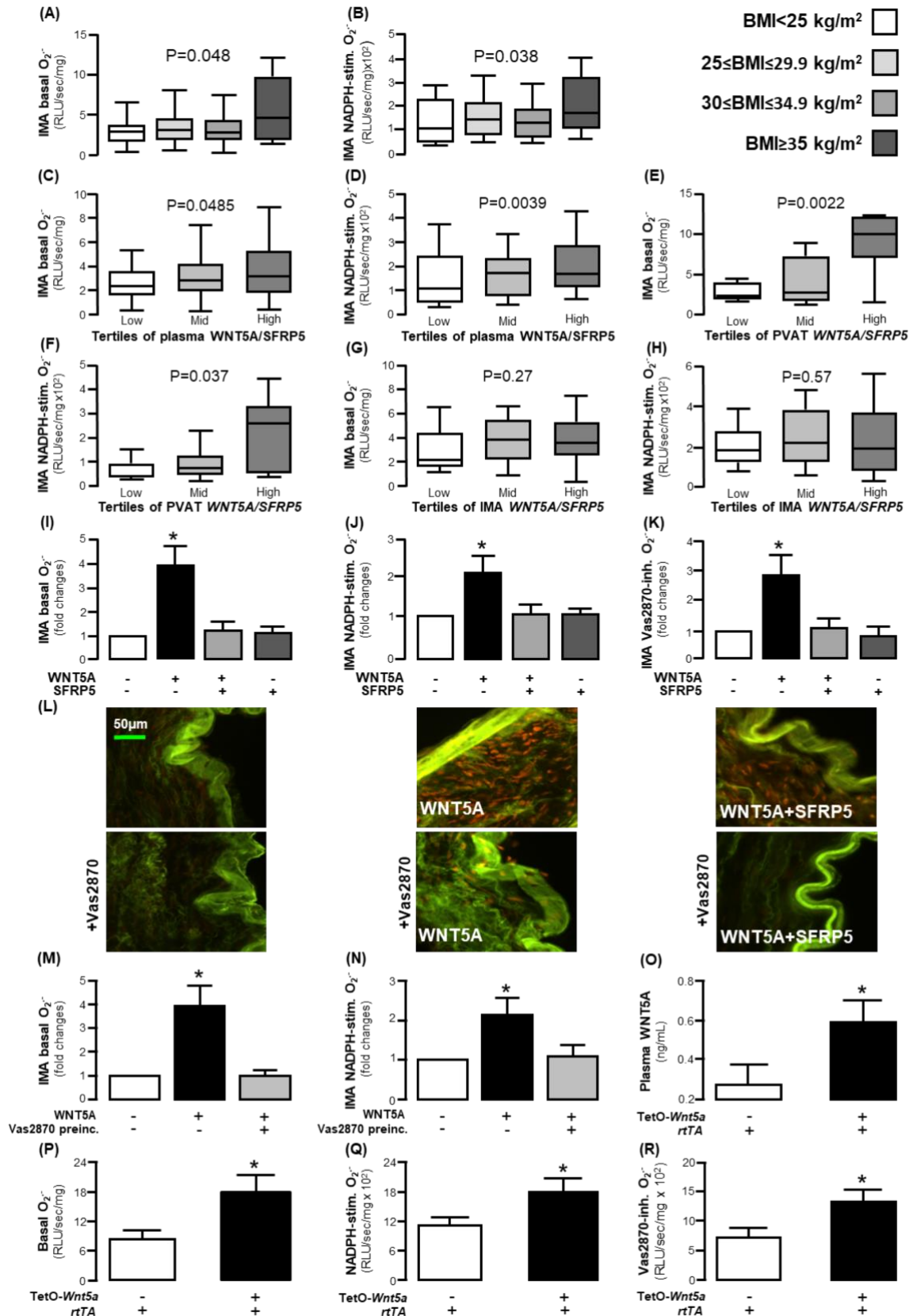
Fig. 3. WNT5A regulates vascular redox state in humans. (**A**) Basal and (**B**) NADPH-

stimulated superoxide ($O_2^{.-}$) production in internal mammary artery (IMA) segments according

to BMI (study 1). (**C**) Basal and (**D**) NADPH-stimulated $O_2^{.-}$ production in IMAs according to circulating plasma WNT5A/SFRP5 ratio tertiles. (**E**) Basal and (**F**) NADPH-stimulated $O_2^{.-}$ production in IMAs according to *WNT5A/SFRP5* ratio tertiles in perivascular adipose tissue (PVAT). (**G**) Basal and (**H**) NADPH-stimulated $O_2^{.-}$ production in IMAs according to *WNT5A/SFRP5* ratio tertiles in internal mammary arteries (IMAs). (**I**) Basal, (**J**) NADPH-stimulated, and (**K**) Vas2870-inhibitable $O_2^{.-}$ production in IMAs in the presence and absence of WNT5A and SFRP5 in ex vivo IMA segments (*n* =5-10 pairs per intervention). (**L**) Dihydorethidium (DHE) staining in IMAs incubated with or without Vas2870 , WNT5A, and SFRP5 (specific oxidised DHE fluorescence corresponds to the red signal; the green signal reflects tissue autofluorescence). (**M**) Basal or (**N**) NADPH-stimulated $O_2^{.-}$ production in IMAs in pre-incubated (preinc.) with Vas2870 and treated with WNT5A (*n* = 5-10 pairs per intervention). (**O**) Circulating plasma WNT5A (n = 11-14 mice per group) and (**P**) basal $O_2^{.-}$, (**Q**) NADPH-stimulated $O_2^{.-}$, and (**R**) Vas2870-inhibitable $O_2^{.-}$ in TetOWNT5A mouse aortae (O: *n* = 5 per group, P-R: *n* = 7 per group). Data are presented as median[25_{th}-75_{th} percentile] (A-H) or as mean ± SEM (I-K, N-R). *P* values in (A-H) are calculated by Kruskal Wallis tests; *$P < 0.05$ vs control in (I-J) and (M-N) by Wilcoxon signed-rank tests; *P* values are calculated by Mann Whitney U tests in (O-R).
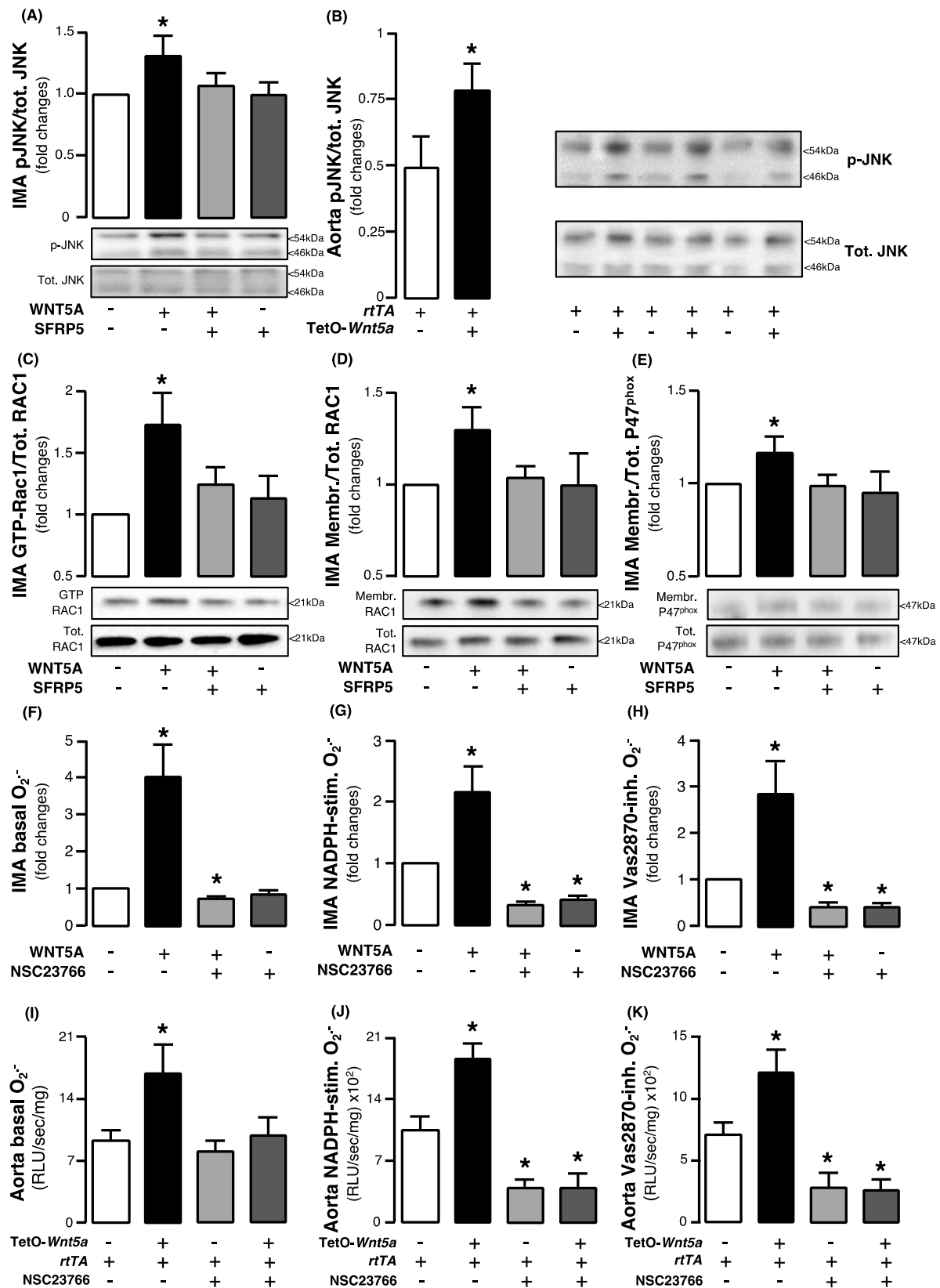
Fig. 4. WNT5A triggers RAC1activation, resulting in NADPH oxidases in the human vascular wall. Fold change of phosphorylated c-jun N-terminal kinase (JNK) in (**A**) human

internal mammary artery (IMA) segments ex vivo (n=5 of paired samples)) in the presence

and absence of WNT5A and SFRP5 and in (**B**) *Wnt5a+/rtTA+* mouse aortae in vivo ($n = 5$ per

group. (**C**) Activation of RAC1 and membrane translocation of (**D**) RAC1 and (**E**) P47phox

subunits of NADPH oxidases in human IMAs ($n = 5$ of paired samples) ex vivo in the presence

or absence of WNT5A and SFRP5. (**F**) Basal, (**G**) NADPH-stimulated, and (**H**) Vas2870-

inhibitable superoxide ($O_{2.-}$) anion production in IMA segments with or without WNT5A and

NSC23766, a specific RAC1 inhibitor ($n = 8$-10 pairs per intervention). (**I**) Basal, (**J**) NADPH-

stimulated, and (**K**) Vas2870-inhibitable superoxide ($O_{2.-}$) anion production in *Wnt5a+/rtTA+*

mouse aortae incubated with or without WNT5A and NSC23766 ($n = 5$-7 per group). Data are

presented as mean $\pm$ SEM.*$P < 0.05$ vs control in all panels by Wilcoxon signed rank tests.

SEM: Standard error of the mean.
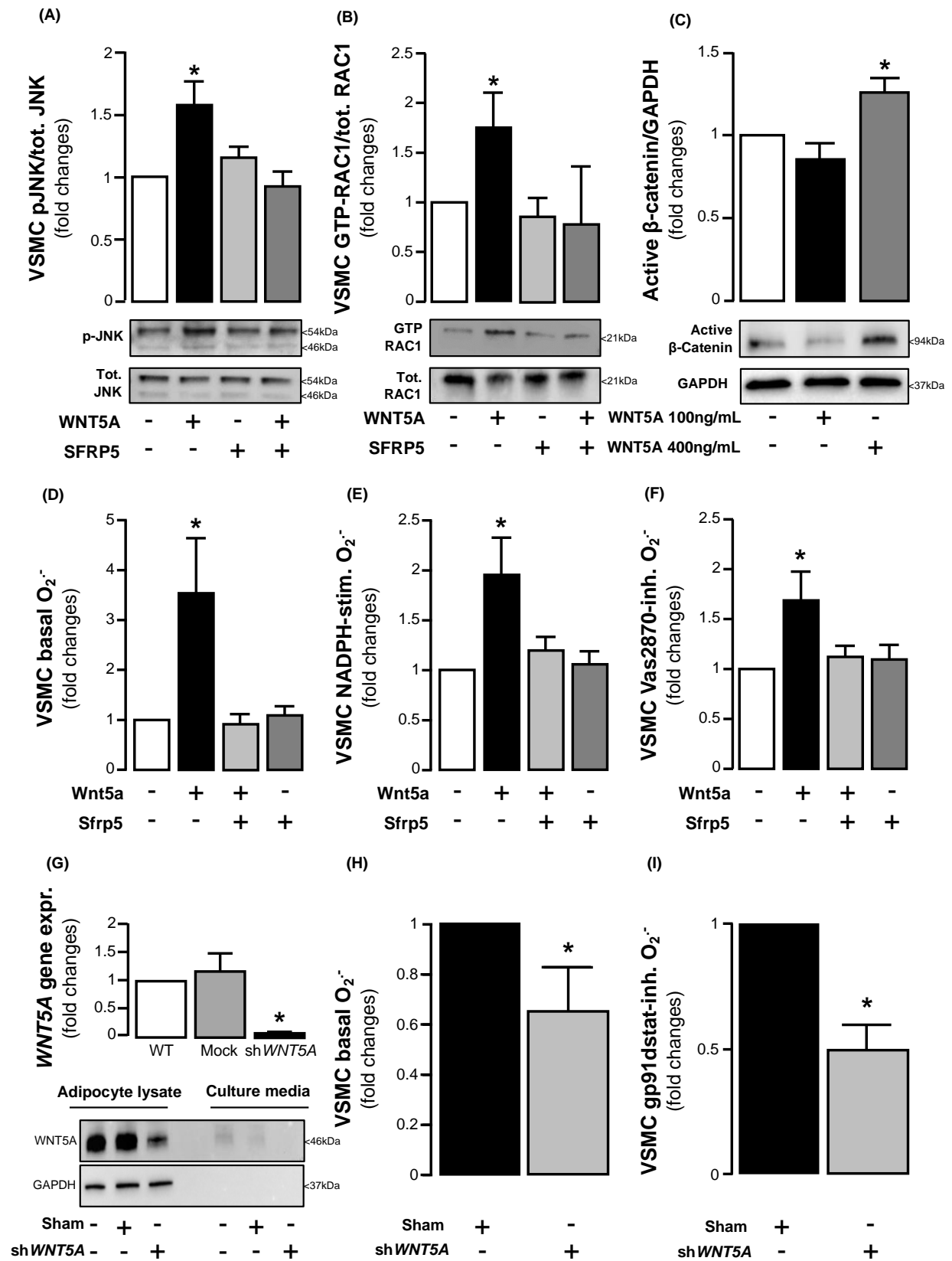
Fig. 5. WNT5A is secreted by adipocytes and enhances NADPH oxidase activity in human vascular smooth muscle cells via RAC1 activation. Fold change of (**A**) phosphorylated c-

Jun N-terminal kinase (JNK) ($n = 5$), (**B**) activated RAC1 ($n = 5$), and (**C**) activated β-catenin ($n = 6$) in VSMCs in the presence or absence of WNT5A and SFRP5. (**D**) Basal, (**E**) NADPH-stimulated, and (**F**) Vas2870-inhibitable superoxide ($O_{2.-}$) production in VSMCs ($n = 6\text{-}11$ pairs per intervention) in the presence or absence of WNT5A and SFRP5. (**G**) Knock-down of *WNT5A* in human immortalised pre-adipocytes ($n = 3$). (**H**) Basal and (**I**) gp91 dstat-inhibitable $O_{2.-}$ production in VSMCs co-cultured with or without *WNT5A*-KO preadipocytes displayed lower ($n = 5$). Data are presented as mean ± SEM *$P < 0.05$ vs control by Wilcoxon signed ranks tests (A-F, H-I) or paired t-test (G). SEM: Standard error of the mean.
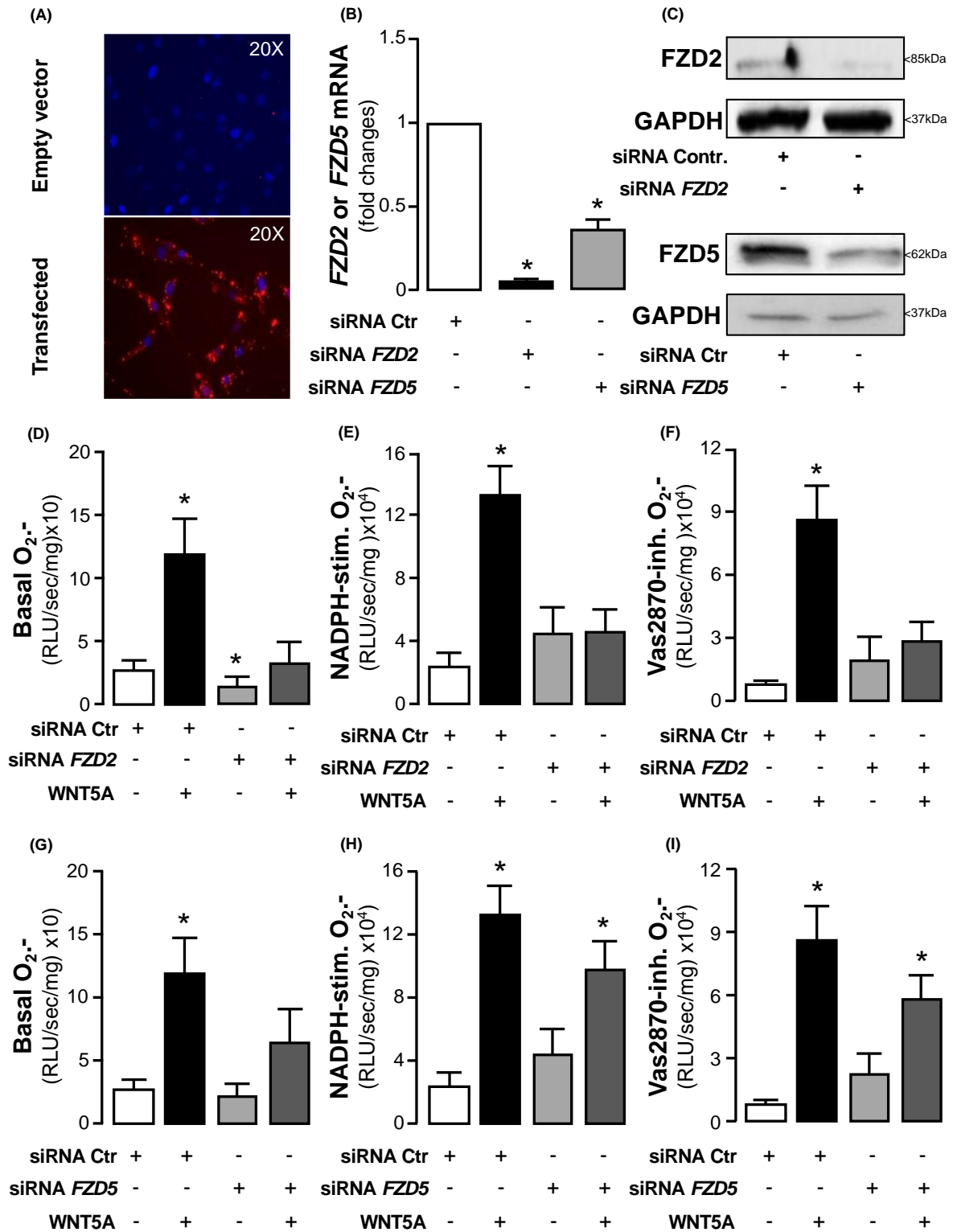
Fig. 6. The pro-oxidant effects of WNT5A in human vascular smooth muscle cells are mediated by Frizzled 2 (Fzd2) and Frizzled 5 (Fzd5) receptors. (**A**) Fluorescence lipofectamine RNAimax imaging (BLOCK-iT Alexa Fluor Red Fluorescence) against cell

nuclei stained with DAPI (blue signal), (**B**) fexpression old change, and (**C**) Western blotting of transfection efficiency of knock-down of *FZD2* and *FZD5* genes in VSMCs (~96% downregulation of *FZD2,* ~65% downregulation of *FZD5; n* = 3). (**D**) Basal, (**E**) NADPH-stimulated, and (**F**) Vas2870-inhibitable $O_{2.-}$ production in siRNA-*FZD2*-treated VSMCs (*n* = 5-6 pairs per intervention) in the presence or absence of WNT5A. (**G**) Basal, (**H**) NADPH-stimulated, and (**I**) Vas2870-inhibitable $O_{2.-}$ production in siRNA-*FZD5*-treated VSMCs (*n* = 6 pairs per intervention) in the presence or absence of WNT5A. Data are presented as mean ± SEM. *P < 0.05 vs control by Wilcoxon signed ranks tests (D-I) or paired t-test (B). SEM: Standard error of the mean.
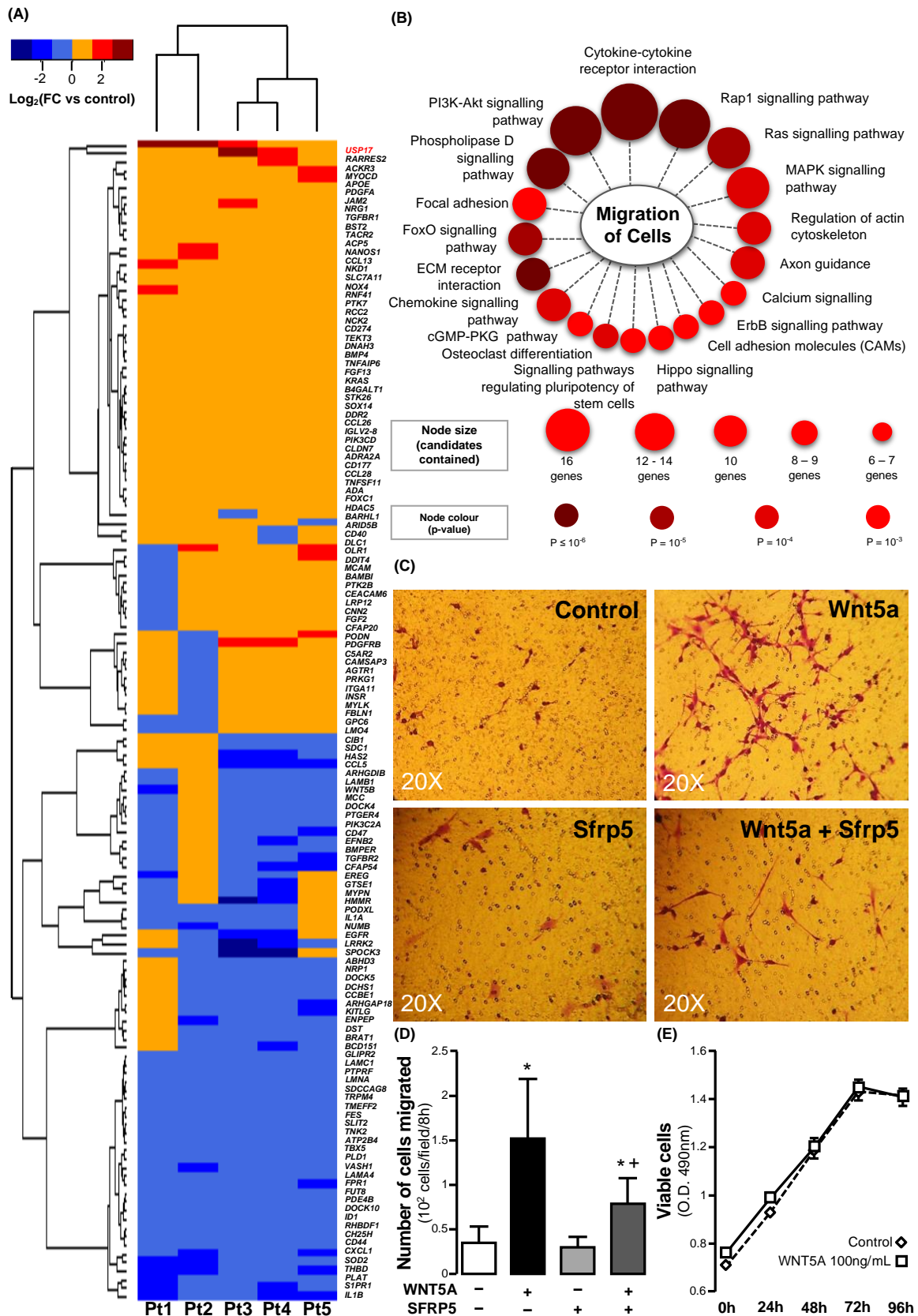
Fig. 7. WNT5A **triggers redox-dependent migration of human vascular smooth muscle**

cells. (**A**) Hierarchical clustering of 136 WNT5A differentially expressed genes (DEGs, Fold

change > 1 or < -1, $P \leq 0.05$) in WNT5A -treated VSMCs from $n = 5$ patients. DEGs were annotated with cell motility function in Gene Ontology (GO) database. (**B**) Enriched signaling pathways of WNT5A cell-motility DEGs identified through ConsensusPathDB. (**C**) Microscopy and (**D**) quantitation of Boyden chamber assay for cell migration, using VSMCs treated with or without recombinant WNT5A and SFRP5 ($n = 30$). (**E**) Proliferation of VSMCs in the presence of WNT5A ($n = 6$-9 per time point per group, evaluated by two-way ANOVA for repeated measures). Data are presented as mean ± SEM in panels D-E. *$P < 0.05$ vs control by Wilcoxon signed rank tests; +$P < 0.05$ vs WNT5A by Wilcoxon signed rank test. SEM: Standard error of the mean; FC: Fold change.
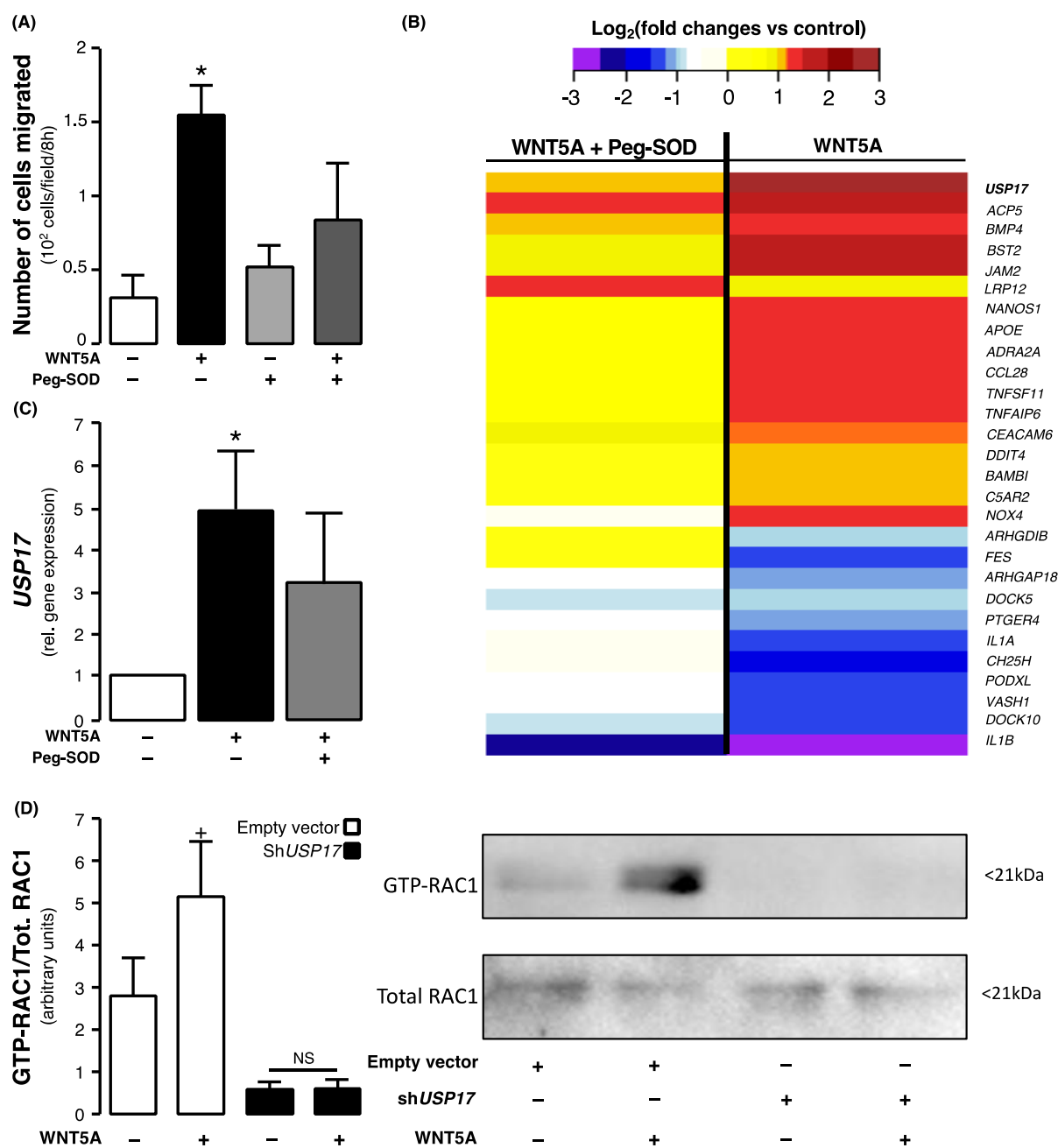
Fig. 8. USP17 as a link between WNT5A and vascular redox signaling. (A) Migration of

VSMCs incubated with peg-SOD, an intracellular scavenger of superoxide ($O_{2.-}$) production,

(n = 5-8 pairs per intervention) and treated with WNT5A. **(B)** A subset of the WNT5A cell-

motility differentially expressed genes of the microarray analysis were at least partially rescued

by superoxide ($O_{2.-}$) anion scavenging with superoxide dismutase (peg-SOD) resulting in p-

values>0.05 (n = 5 pairs, genes presented by descending mean fold change). **(C)** USP17

expression in VSMCs incubated with peg-SOD and treated with WNT5A ($n = 10$). (**D**) RAC1 activation in HeLa cells transfected with shUSP17 and treated with WNT5A ($n = 8$). Data are presented as mean ± SEM in panels A, C and D. *$P < 0.05$ vs control by Wilcoxon signed rank test in panels A & C.+$P<0.05$ vs untreated empty vector control by Wilcoxon signed rank test; NS by Wilcoxon signed rank test for WNT5A -treated vs untreated sh*USP17* cells in panel D.

Supplementary Material

Adipose tissue-derived WNT5A regulates vascular redox signalling in obesity via USP17/Rac1-mediated activation of NADPH oxidases

Ioannis Akoumianakis[1], Fabio Sanna[1], Marios Margaritis[1], Ileana Badi[1], Nadia Akawi[1], Laura Herdman[1], Patricia Coutinho[1], Harry Fagan[1], Alexios S Antonopoulos[1], Evangelos K Oikonomou[1], Sheena Thomas[1], Amy P Chiu[1], Surawee Chuaiphichai[1], Christos P Kotanidis[1], Constantinos Christodoulides[3], Mario Petrou[2], George Krasopoulos[2], Rana Sayeed[2], Lei Lv[1], Ashley Hale[1], Meisam Naeimi Kararoudi[1], Eileen McNeill[1], Gillian Douglas[1], Sarah George[4], Dimitris Tousoulis[5], Keith M Channon[1], Charalambos Antoniades[1]*

[1]Division of Cardiovascular Medicine, University of Oxford, Oxford, UK

[2]Department of Cardiothoracic Surgery, Oxford University Hospitals NHS Trust, Oxford, UK

[3]Oxford Centre for Diabetes, Endocrinology and Metabolism, University of Oxford, Oxford, UK

[4]Bristol Medical School, Research Floor Level 7, Bristol Royal Infirmary, Bristol, UK

[5]Cardiology Department, Athens University Medical School, Athens, Greece

I. A. and F. S. contributed equally to this study.

*Corresponding author:
Charalambos Antoniades MD PhD FESC
Professor of Cardiovascular Medicine University of Oxford
Division of Cardiovascular Medicine, L6 West Wing, John Radcliffe Hospital,
Headley Way, Oxford OX3 9DU, UK
e-mail: antoniad@well.ox.ac.uk
Tel: +441865228340
Fax: +44186534615

Supplementary methods

In vitro studies

Primary vascular smooth muscle cell (VSMC) isolation & characterisation

Human saphenous vein (SV) explants from 46 patients (38 males, 8 females) were washed in phosphate-buffered saline (PBS) and the adventitia layer was removed. Vessels were cut longitudinally to expose the endothelium, which was removed using a scalpel. The tissue was washed in PBS and digested with 0.25% trypsin for 10min. The digested tissue was diced into 1mm2 sections and seeded in Dulbecco's modified eagle media (DMEM)+20% FBS. VSMCs were grown in Media 231 supplemented with smooth muscle growing supplement (SMGS) (Life Technologies Ltd) in a cell culture incubator at 37oC and 5% CO_2 following the first passage.

For characterisation purposes, VSMCs were plated on a 6-well plate for 24h, culture media was removed and cells fwere ixed with 4% paraformaldehyde. To permeabilise the cells, 0.2% Triton in PBS was added for 10min at room temperature and the cells were then washed thrice with PBS and blocked with 10% bovine serum albumin (BSA). Cells were incubated overnight at 4°C with mouse monoclonal anti-CD31 (Sigma, P8590) or mouse monoclonal anti-α-smooth muscle actin (Sigma, A5228) primary antibody and secondary antibody goat-anti mouse Alexa Fluor 488 conjugated (ab150113, Abcam) for 1 hour at room temperature. Following 3 washes with PBS, the cells were dried and mounted with Slow Fade Gold Anti Fade with DAPI (S36939, ThermoFisher) before visualization with fluorescence inverted microscope (Olympus IX71, fig. S6).

Co-culture experiments

VSMCs were co-cultured with human pre-adipocytes using trans-well plate (0.4 µm polycarbonate filter, Corning) for 24 h. Human pre-adipocytes were cultured in the bottom chamber and VSMCs in the top one.

Cell proliferation assay

1×10^4 cells per well were seeded in a 96 well plate in 100 µL of culture medium and grown at 37 °C in the presence or absence of WNT5A 100 ng/mL or SFRP5 300 ng/mL. At the indicated incubation time points (24, 48, and 72 h), 20 µL CellTiter 96 AQueous One Solution Reagent (Promega) was added to each well and the plates were incubated for 2 h at 37 °C. Subsequently, absorbance at 490 nm was measured using a 96-well plate reader, which served as an indicator of the number of viable cells in each well.

Cell migration assay

Cell migration was assessed in a modified Boyden chamber (Costar), in which two chambers were separated by a polycarbonate membrane (pore diameter, 8.0 µm). VSMCs were grown overnight in serum-free medium-231; the following day, 3×10^4 cells were seeded into the trans-wells with a membrane placed in the bottom. Medium-231 containing 0.1% FBS and different interventions: 100 ng/mL WNT5A, 300 ng/mL SFRP5and 100 IU/mL pegylated superoxide dismutase (peg-SOD, Sigma) was added to both the upper and lower compartment of the Boyden chamber. The cells were allowed to migrate for 8 h at 37°C in this setting. Thereafter, medium was discarded, cells were fixed with 4% paraformaldehyde (PFA) and stationary cells removed with a cotton bud. Cells were stained with 0.5% crystal violet and the number of cells having migrated through the membrane was evaluated in a light microscope by cell counting. Considering that WNT5A (and all other interventions) were present in both compartments of the Boyden chamber at equal concentrations, these results should be

interpreted in the context of the ability of WNT5A to stimulate the motility and migration capacity of VSMCs, not its ability to act as a chemoattractant.

Wound Healing assay

VSMCs were trypsinized and re-suspended in PBS to a concentration of $5x10^5$ cells/mL. 70 µL of cell suspensions were added to each chamber of the ibidi Culture-Insert (cat. IB-81176), where cells were allowed to grow until confluency. The plastic insert was removed after 24h of serum starvation and, medium was replaced with DMEM containing 0.1% fetal bovine serum (FBS) following two washes with PBS and cellular monolayers were allowed to heal for 15 h. Photographs of central wound edges per condition were taken at time zero and at the indicated time points using a digital camera.

VSMC phenotypic switch

VSMCs were treated with recombinant WNT5A 100ng/mL or vehicle for 8h following overnight serum starvation, and contractile-to-synthetic phenotypic switch was evaluated by quantifying the mRNA expression of established markers (smooth muscle α2 actin-ACTA2, transgrelin-TGLN, smooth muscle protein 22α-SM22α, metalloproteinase 9-MMP9 and MMP inhibitors TIMP1 and TIMP2) as described below.

Transfection studies with Fz2 and Fz5 siRNA

Fzd2, Fzd5 siRNA (ON-TARGET plus SMART pool) and negative control siRNA (ON-TARGET plus non-targeting pool) were purchased from Dharmacon and used to knock-down Fzd2 and Fzd5 receptors in human VSMCs, respectively. Briefly, $1x10^6$ cells were seeded in a 6 well plate for 24h, and medium was replaced by Optimem on the day of transfection. Lipofectamine RNAiMax (Thermo Fisher Scientific) was used to transfect VSMCs with 100 pmoles of siRNA according to the instructions provided by the manufacturer. 24 h post-transfection, Optimem was replaced by Medium 231 plus SMGS. To test the transfection

ability as well as the toxicity of lipofectamine RNAiMax on primary VSMCs, BlockiT Alexa Fluor Red Fluorescent control (14750100, ThermoFisher) was used as positive transfection control.

Transfection studies with shUSP17

HeLa cells from passage 10-17 were cultured in growth medium DMEM with 10% FCS, 1% penicillin/streptomycin, and 200 mM L-glutamine at 37 °C in a 5% CO_2 humidified incubator. Cells were starved overnight, and transfected with pRS-USP17 shRNA (TG321147, Origene Technologies) using FuGENE6 (E2691, Promega).

Total RNA was isolated using Trizol, followed by chloroform and isopropanol extraction, washing by ethanol and dissolving in DEPC-H_2O. USP17 mRNA expression was detected as described previously (*18*). Briefly, 1 µg total RNA was applied using the OneStep RT–PCR kit (210210, Qiagen). The primer sets for USP17 are:

 5′-CAGTGAATTCGTGGGAATGGAGGACGACTCACTCTAC-3′ (forward)

5-AGTCATCGATCTGGCACACAAGCATAGCCCTC-3′ (reverse)

We used β-actin as a housekeeping gene by the following primers:

5′-GGACTTCGAGCAAGAGATGG-3′ (forward)

5′-AGCACTGTGTTGGCGTACAG-3′ (reverse)

Clones with undetectable USP17 expression were used for 8h incubations with WNT5A 100ng/mL and Rac1 activation was assessed compared to transfection controls.

Coronary calcium score (CCS) quantification in study 3

At both time points (baseline and follow-up) a non-contrast prospectively ECG-triggered axial acquisition CT scan was obtained (2.5-3.0 mm axial slice thickness, tube energy of 120 kV) with the carina and the diaphragm used as cranial and caudal landmarks respectively. In all patients, the baseline scan was acquired using a 64-slice LightSpeed Ultra CT scanner (General Electric Healthcare), whereas all follow-up scans were performed in a 320-slice Aquilion One scanner (Toshiba Medical Systems). CCS was measured on a dedicated workstation (Aquarius Workstation V.4.4.13, TeraRecon Inc., Foster City) according to the Agatston method (*41*). Coronary calcification progression was defined as any change in CCS ≥ 1, while new onset calcification was evaluated in those patients having CCS=0 at the time of the baseline scan.

Ex Vivo incubations of human vascular tissue

All ex vivo incubations of human tissue were performed as we have previously described (*40,43*). Fresh, intact human IMA samples were cut into sequential rings and opened longitudinally to expose the endothelial surface. Each segment was then equilibrated for 45 minutes in oxygenated (95% O_2/5% CO_2) Krebs-HEPES buffer (pH 7.4) at 37°C, where carrier (sterile PBS), WNT5A 100ng/mL (R&D Systems, 645-WN/CF) or SFRP5300ng/mL (R&D Systems, 6266-SF) was added. The vascular segments were then used fresh for superoxide ($O_2^{.-}$) quantification or snap-frozen in -80$_o$C until processed later. In a subset of patients, Vas2870 *ex vivo* 20min incubation preceded the WNT5A treatments to pre-inhibit NADPH-oxidases.

For the Rac1 inhibition experiments, human IMA and mouse aortae were pre-incubated with NSC23766 100μM (R&D systems, catalogue number 2161) for 15min prior to any experiment.

For the visualisation of vascular $O_2{}^{.-}$ production, human IMA were incubated in the presence or absence of WNT5A as described earlier, and snap-frozen in optical coherence tomography (OCT) medium until used for oxidative fluorescent microtopography as explained later.

Vasomotor studies

All vasomotor studies were performed as we have previously described (*43*). Briefly, serial SV rings were mounted on Radnotti organ bath chambers and equilibrated for 30 min in $37_{o}C$, 95% O_2/5% CO_2 in Krebs Henseleit buffer (NaCl 120 mM, KCl 4.7 mM, $CaCl_2$ 2.5 mM, $MgSO_4$ 1.2 mM, KH_2PO_4 1.2 mM, $NaHCO_3$ 25 mM, glucose 5.5 mM, pH = 7.4). Endothelial function was assessed by endothelium-dependent, acetylcholine (ACh)-mediated dose-response relaxations (10_{-9} M to $3\times10_{-6}$ M) after phenylephrine (PE) $3\times10_{-6}$ M pre-constriction. Endothelium-independent vasorelaxations were also evaluated in the same rings after in-chamber eNOS inhibition (by LNAME), and endothelium-independent vasorelaxations were evaluated by sodium nitroprusside (SNP, 10_{-10} M to 10_{-6} M). All *ex vivo* incubations (WNT5A 100 ng/mL and/or SFRP5 300 ng/mL) were performed in the organ bath chambers for 45min prior to dose response curves. All results are expressed as percentages of the PE pre-constriction.

Superoxide Measurements

Primary VSMCs

Production of $O_2{}^{.-}$ was measured using a lucigenin (5 µmol/L)-enhanced chemiluminescence assay as we have previously described (*40*). VSMCs were incubated with WNT5A 100 ng/mL or SFRP5300 ng/mL for 30 min, then scraped in ice-cold buffer (KH_2PO_4 50mM, EGTA 1

mM, sucrose 150 mM, pH = 7) in the presence of a protease inhibitor cocktail (Roche Applied Science) and lysed using an ultrasound bath. The contribution of NADPH-oxidases activity to the production of O_2^- was quantified in the presence of NADPH 400 µmol/L (NADPH-stimulated O_2^-). Vas2870 (a specific pan-NADPH-oxidases inhibitor (*40*)) was also used to quantify the Vas2870-inhibitable O_2^- as a more specific index of NADPH-oxidases activity. Vas2870 was routinely used as part of the standard assay procedure to improve the specificity of the technique towards NADPH-oxidases, not as a biological incubation.

Vascular tissue

Vascular O_2^- production was routinely measured in fresh, intact human IMA and in selected mouse aorta segments by using lucigenin (5 µmol/L)-enhanced chemiluminescence, as we have described previously (*40, 43*). Vessels were opened longitudinally to expose the endothelial surface and equilibrated for 20 minutes in oxygenated (95% O_2/5% CO_2) Krebs-HEPES buffer (pH=7.4) at 37°C. The contribution of NADPH-oxidases activity to the production of O_2^- was evaluated in the presence of NADPH 100 µmol/L and by quantifying the Vas2870-inhibitable O_2^-. The Pan-NOX inhibitor Vas2870 was routinely used as part of the standard assay procedure to define the specific fraction of the chemiluminescence signal derived from NOXs, improving the specificity of the technique towards NADPH-oxidases, as we have previously described (*40, 43*). In a specific experiment aiming to test whether the effect of WNT5A on vascular O_2^- is conditional upon activation of NADPH-oxidases, the human arterial segments were pre-incubated with Vas2870 prior to exposure to WNT5A, as part of the actual experimental design, as clearly stated in relevant sections.

The coupling status of eNOS was assessed by quantification of the difference in arterial O_2^- generation before and after addition of N(G)-Nitro-L-arginine methyl ester (LNAME, 1mM). LNAME is an eNOS inhibitor, therefore reduction of vascular O_2^- after LNAME incubation suggests that eNOS is a source of O_2^- (therefore predominantly uncoupled), while increase of

$O_2^{.-}$ following inhibition of eNOS by LNAME, suggests that the enzyme is largely coupled, producing NO (which is a scavenger of $O_2^{.-}$). The LNAME-inhibitable $O_2^{.-}$ is therefore a measure of eNOS uncoupling, as we have described in the past (*43, 44*).

Oxidative fluorescent microtopography

In situ $O_2^{.-}$ production was determined in vessel cryosections with oxidative fluorescent dye dihydroethidium (DHE), as we have previously described (*43*). Serial IMA rings from n=4 patients were incubated with/without WNT5A 100 ng/ml for 45 minutes and subsequently snap frozen in OCT. Cryosections (30 μm) were incubated with DHE (2 μmol/L for 5 minutes) in Kreps-Hepes buffer, with or without Vas2870 (400 μmol/L). Fluorescence images of the endothelium (x63, Zeiss LSM 510 META laser scanning confocal microscope) were obtained from each vessel quadrant. In each case, segments of vessel rings (± Vas2870) were analysed in parallel with identical imaging parameters in a blinded fashion.

Arterial biopterin measurements

Vascular BH4, BH2 and biopterin (B) content was quantified by HPLC followed by electrochemical (for BH4) and fluorescent (for BH2 and B) detection, as we have previously described (*44, 45*). *Ex vivo* incubated IMA rings were subjected to 3 freeze/thaw cycles in re-suspension buffer (50 mM phosphate buffered saline, 1 mM Dithioerythritol (DTE), 1mM EDTA, pH=7.4) to induce endothelial cell lysis, debris was removed, and supernatant proteins were precipitated with ice-cold precipitation buffer (H3PO4 1M, trichloroacetic acid (TCA) 2M and DTE 1mM). Samples were injected onto an HPLC system and quantified using sequential electrochemical and fluorescence detection. Quantification of BH4, BH2 and B was

by comparison with external standards (1nM – 0.1μM) prepared from 10 μM BH4, BH2 and B (Schircks, Zurich) stocks with serial dilutions in ice-cold re-suspension buffer.

RNA Isolation, Reverse Transcription and Quantitative Real Time-Polymerase Chain Reaction (qRT-PCR)

RNA isolation

Total RNA was isolated by phenol:chloroform (1:5 ratio) separation followed by magnetic beads-based RNA purification on a KingFischer magnetic particle processor (Thermo Fischer Scientific) by using the MagMAX mirVana total RNA isolation kit (Thermo Fischer Scientific, Catalogue Number A27828). RNA concentration and quality was evaluated spectrophotometrically on NanoDrop ND-1000.

Reverse transcription

RNA was reverse-transcribed to cDNA by using SuperScript VILO mastermix (Thermo Fischer Scientific) following the Manufacturer's instructions and extending the cDNA synthesis step to two hours at 60_oC on a Veriti thermal cycler (ABI).

Quantitative real-time PCR

Quantitative real-time PCR was performed by TaqMan chemistry, using the standard universal TaqMan protocol as indicated by the Manufacturer, on a QuantStudio 7 flex real-time PCR system (Thermo Fischer Scientific). All samples were run in duplicates using 5 ng of cDNA as starting mass, and data was analysed by the Pfaffl method (*46*). Cyclophilin A (PPIA) was used as housekeeping gene for human AT and pre-adipocytes, while GAPDH was used as housekeeping gene for human vascular tissue and VSMCs.18S ribosomal RNA was used as housekeeping for mouse samples. The IDs of the TaqMan probes used are:

PPIA: Hs99999904_m1; *GAPDH*: Hs02786624_g1; *SFRP5*: Hs00169366_m1; *WNT5A*: Hs00998537_m1; *WNT5B*: Hs01086864_m1; *WNT1*: Hs00180529_m1; *WNT3A*: Hs00263977_m1; *WNT3*: Hs00902257_m1; *WNT9A*: Hs01573829_m1; *WNT9B*: Hs00287409_m1; *WNT10A*: Hs00228741_m1; *WNT10B*: Hs00928823_m1; *WNT11*: Hs01045906_m1; *WNT6*: Hs00362452_m1; *WNT4*: Hs01573505_m1; *WNT2*: Hs00608224_m1; *WNT16*: Hs00365138_m1; *WNT2B*: Hs00921614_m1; *WNT7A*: Hs01114990_m1; *WNT7B*: Hs00536497_m1; *WNT8A*: Hs00230534_m1; *WNT8B*: Hs00610126_m1; *FZD2*: Hs00361432_s1; *FZD5*: Hs00258278_s1; *ROR1*: Hs00938677_m1; *ROR2*: Hs00896176_m1; *RYK*: Hs00243196_m1; *USP17*: Hs00970729_g1; *ACTA2*: Hs05005341_m1; *TAGLN:* Hs01038780_m1; *MMP9:* Hs00957562_m1; *TIMP1:* Hs01092511_m1; *TIMP2:* Hs00234278_m1; *NOX1:* Hs01071088_m1; *NOX2:* Hs00166163_m1; *NOX4:* Hs01379108_m1; *NOX5:* Hs00225846_m1; *WNT5A*: Mm00437347_m1; *18S RNA*: Mm04277571_s1

Sample Preparation for Western Blotting

Cell culture

Protein extracts were obtained from 80% confluent cells, which were washed in cold PBS and lysed in RIPA buffer (Cell Signalling) containing proteases and phosphatases inhibitors (Roche). Protein concentrations were determined using the BCA assay (Pierce), with albumin as standard.

Vascular tissue processing

Human IMA segments and mouse aortic tissue were homogenised in ice-cold RIPA buffer (Cell Signalling) supplemented with proteases and phosphatases inhibitors (Roche) by using a TissueLyser LT (Qiagen). Protein concentrations were determined using the BCA assay (Pierce), with albumin as standard.

Western blotting

20µg of denatured protein extracts were analysed by SDS/PAGE on 4-20% polyacrylamide gradient gel, and the proteins were then transferred to nitrocellulose membranes (Amersham). For detection of immuno-reactive bands, ECL select Western Blotting Detection Reagent (Amersham) was used. Western blots were quantified using Image Lab Bio-rad software integrated density analysis. The primary antibodies used were: rabbit polyclonal anti-Nox1 (ab131088, Abcam, 1:1,000), rabbit monoclonal anti-Nox2 (EPR6991, Abcam, 1:5,000), rabbit monoclonal anti-Nox4 (ab109225, Abcam, 1:1,000), anti-anti-Nox5 (HPA019362, Sigma, 1:1,000), rabbit monoclonal anti p-SAPK/JNK (Thr183/Tyr185) (4671, Cell Signalling, 1:500), rabbit monoclonal anti-SAPK/JNK (9258, Cell Signalling, 1:500), rabbit polyclonal anti-frizzled 2 (Abcam, ab52565, 1:1,000), rabbit polyclonal anti-frizzled 5 (06-756, Millipore, 1:1,000), rabbit monoclonal anti- WNT5A (C27E8, Cell Signalling, 1:1,000) mouse monoclonal anti-active β catenin (05-665, Millipore, 1;1,000) and mouse anti-GAPDH HRP-conjugated (G9295, Sigma 1:20,000). HRP-conjugated anti-rabbit (A9169, Sigma, 1:10,000) and HRP-conjugated anti-mouse (A9044, Sigma, 1:15,000) were used as secondary antibodies as appropriate.

Rac1 activation assay

Rac1 activation assay was detected using an active rac1 detection kit (Cell Signalling). VSMCs or human IMA segments were lysed or homogenised respectively, using the lysis buffer provided by the kit, supplemented with protease and phosphatase inhibitors. Lysates (500ug) were then incubated with glutathione resin and GST-PAK1-PBD according to the manufacturer's specific instructions (Cell Signalling). Western blot analysis was performed using mouse monoclonal anti-Rac1 (1:1,000) primary antibody and HRP-conjugated anti-mouse (1:15,000) secondary antibody.

shRNA lentiviral particles transduction in immortalised pre-adipocytes

An immortalised human pre-adipocyte cell line from subcutaneous abdominal adipose tissue was kindly donated by Constantinos Christodoulides and Fredrik Karpe, generated as described by Todorčević *et al.* (*47*). Immortalized human pre-adipocytes were cultured in a 6 well-plate until 50% confluence. On the day of the infection, media was replaced with culture media containing 5 µg/mL of hexadimethrine bromide. Immortalized pre-adipocytes were transduced with the appropriate amount of shRNA lentiviral transduction particles to downregulate WNT5A at a multiplicity of infection of 100. 24 h post post-incubation, transduced cells were selected with 0.5 µg/mL puromycin. WNT5A downregulation was then confirmed by qRT-PCR and Western blotting as described in relevant sections.

WNT5A Secretion assay

Human immortalised pre-adipocytes were grown to ∼90% confluence in T75 flasks, washed three times with PBS and cultured with 0.1% BSA. After 24 h, medium was collected and centrifuged at 10,000 g for 10 min. Supernatant was concentrated using Amicon Ultra-15 centrifugal filter system 10KMWCO (Millipore) and centrifuged at 5,000 g at room temperature for 1h and concentrated supernatants were used for Western blotting.

Evaluation of vascular RAC1 and P47$_{phox}$ membrane translocation

Membrane translocation of RAC1 and P47$_{phox}$ in human IMA was estimated by differential centrifugation of vascular homogenates to isolate membrane proteins, and membrane-translocated RAC1 or P47$_{phox}$ protein was determined by Western immunoblotting as we have previously described (*8*). Briefly, vascular segments were homogenized in ice-cold HEPES

buffer (HEPES 20 mM, 150 mM NaCl, and 1 mM EDTA, pH=7.4) supplemented with a protease inhibitor cocktail (Roche, UK). Debris was removed by centrifugation of the homogenates at 2,800 g at 4°C for 20 min, and the protein content of supernatants was evaluated by the Pierce BCA protein assay kit. 500 mg of total protein were adjusted to 200 μL for all samples, added into ultracentrifugation tubes and ultra-centrifuged at 100,000 g for 60 min at 4°C to separate the cytosolic from the membrane proteins. Following removal of supernatants containing the cytosolic proteins, pellets were re-suspended in 35 μL of lysis buffer containing 1% Triton and left for 20 min on ice. Protein concentrations were then quantified, and samples processed for Western immunoblotting as described previously.

Supplementary figures
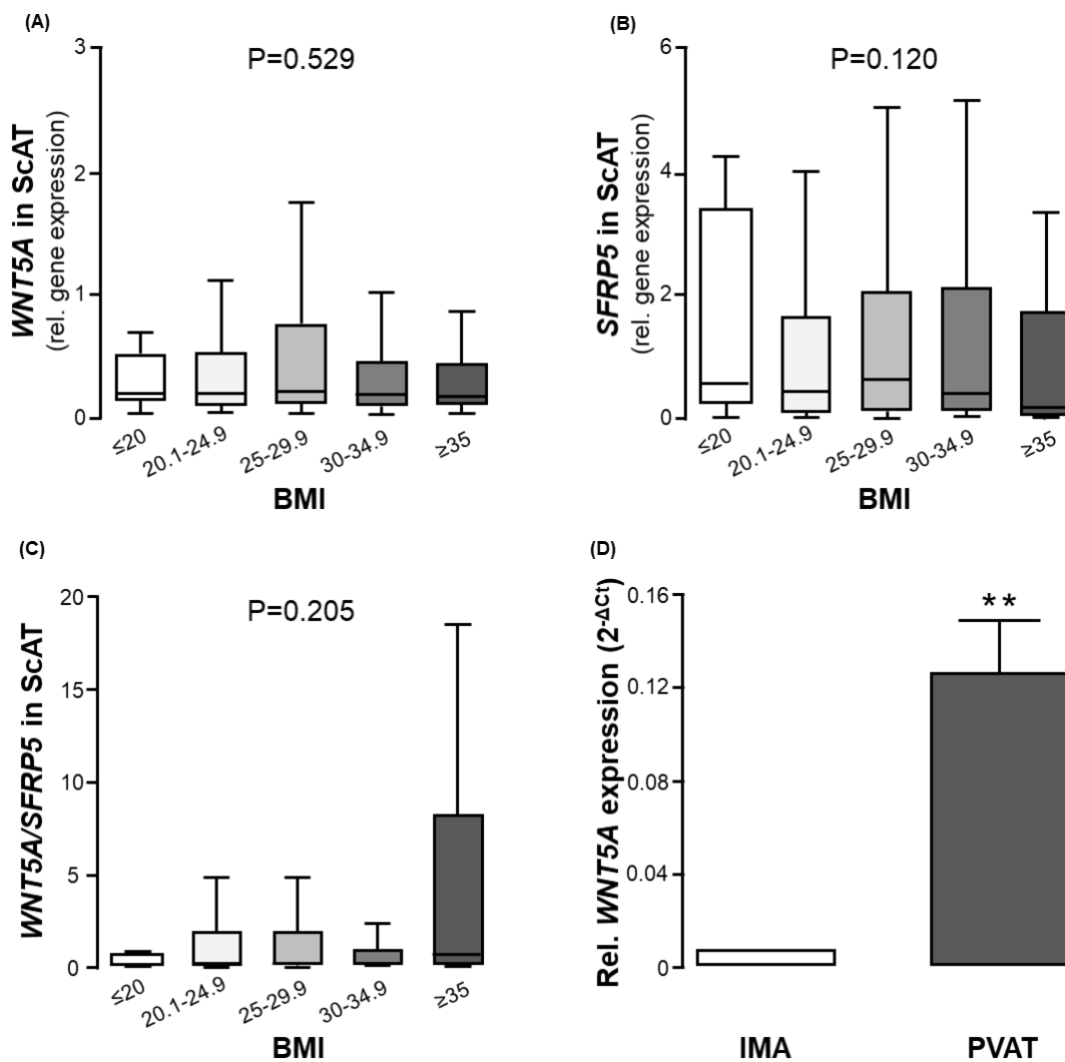
Fig. S1. WNT5A & SFRP5 expression data in subcutaneous adipose tissue (ScAT), internal mammary arteries (IMAs), and perivascular adipose tissue (PVAT). (A-C) The expression of WNT5A (A), SFRP5 (B), and WNT5A/SFRP5 (C) in subcutaneous AT (ScAT) according to BMI (Study 1, n=1,004, data presented as median[25th-75th percentile]). (**D**) The expression of WNT5A in IMAs compared to its expression in PVAT from study 1 (data presented as mean ± SEM). *P* values in (A-C) are calculated by Kruskal Wallis tests; *P* value in (D) is calculated by Man Whitney U test.
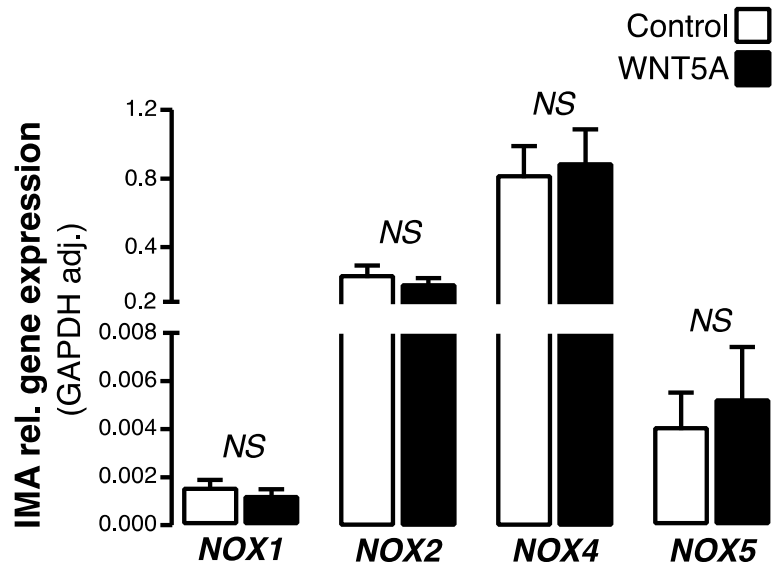
Fig. S2. Ex vivo effect of WNT5A on NOX isoform gene expression in internal mammary arteries (IMA). Gene expression of NOX1, NOX2, NOX4, and NOX5 in internal mammary artery (IMA) segments (n = 5 pairs) with and without 8h ex vivo WNT5A incubation. Data presented as mean ± SEM. P values are calculated by Wilcoxon signed-rank tests.
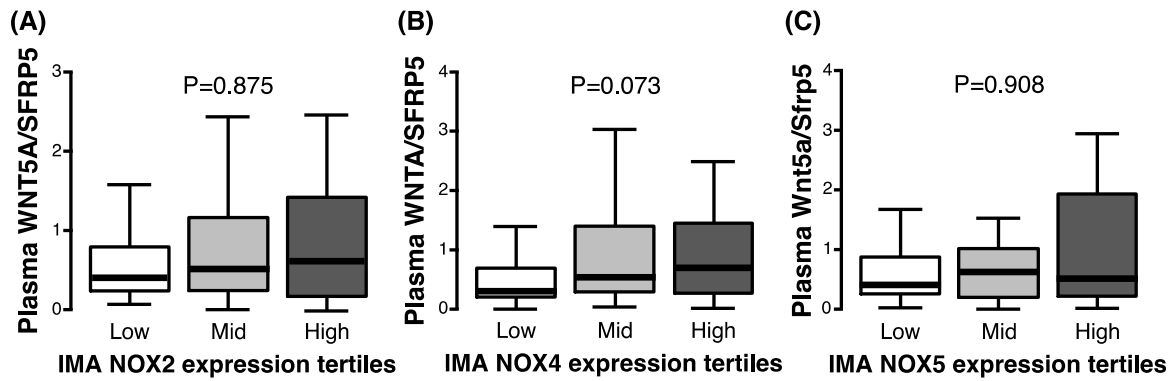
Fig. S3: Association of plasma WNT5A/SFRP5 with arterial *NOX* expression. Circulating WNT5A/SFRP5 ratio according to arterial (internal mammary artery, IMA) expression of **(A)** NOX2, **(B)** NOX4and **(C)** NOX5in study 1. *P* values are calculated by Kruskal Wallis tests; data presented as median[25th-75th percentile].
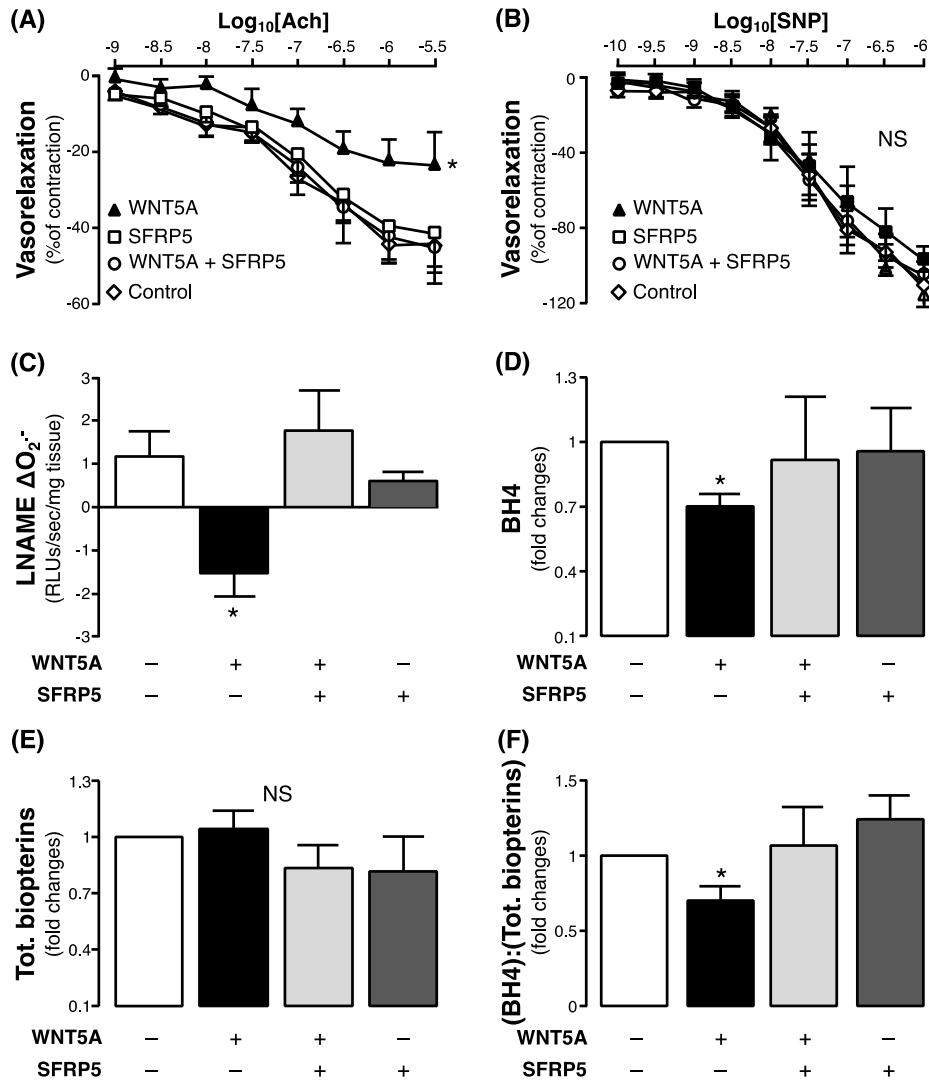
Fig. S4. Effects of WNT5A on endothelial function and endothelial nitric oxide synthase (eNOS) coupling. (**A**) Endothelial nitric oxide (NO) bioavailability in human saphenous veins (SV) ex vivo in the presence of WNT5A and SFRP5, as assessed by acetylcholine (Ach) mediated vasorelaxation and (**B**) endothelium-independent vasorelaxations to sodium nitroprusside (SNP) (n = 3-4 patients per intervention). (**C**) Vascular superoxide O_{2^-} production in human internal mammary artery segments the presence of N(G)-Nitro-L-arginine methyl ester (LNAME) delta(eNOS inhibitor), WNT5A or/and SFRP5, an assay for endothelial nitric oxide synthase (eNOS) uncoupling (n = 4-6 patients per intervention). (**D**) eNOS co-factor tetrahydropterin (BH4), (**E**) total biopterin, and (**F**) BH4/total biopterins ratio in internal mammary artery segments in the presence of WNT5A and SFRP5 (n = 4-5 patients per intervention) . *$P < 0.05$ vs control by two-way ANOVA for repeated measures in (A). Data presented as mean ± SEM. *$P < 0.05$ vs control by Wilcoxon signed-rank tests for (C-F); P value also calculated by two way ANOVA in panel B.
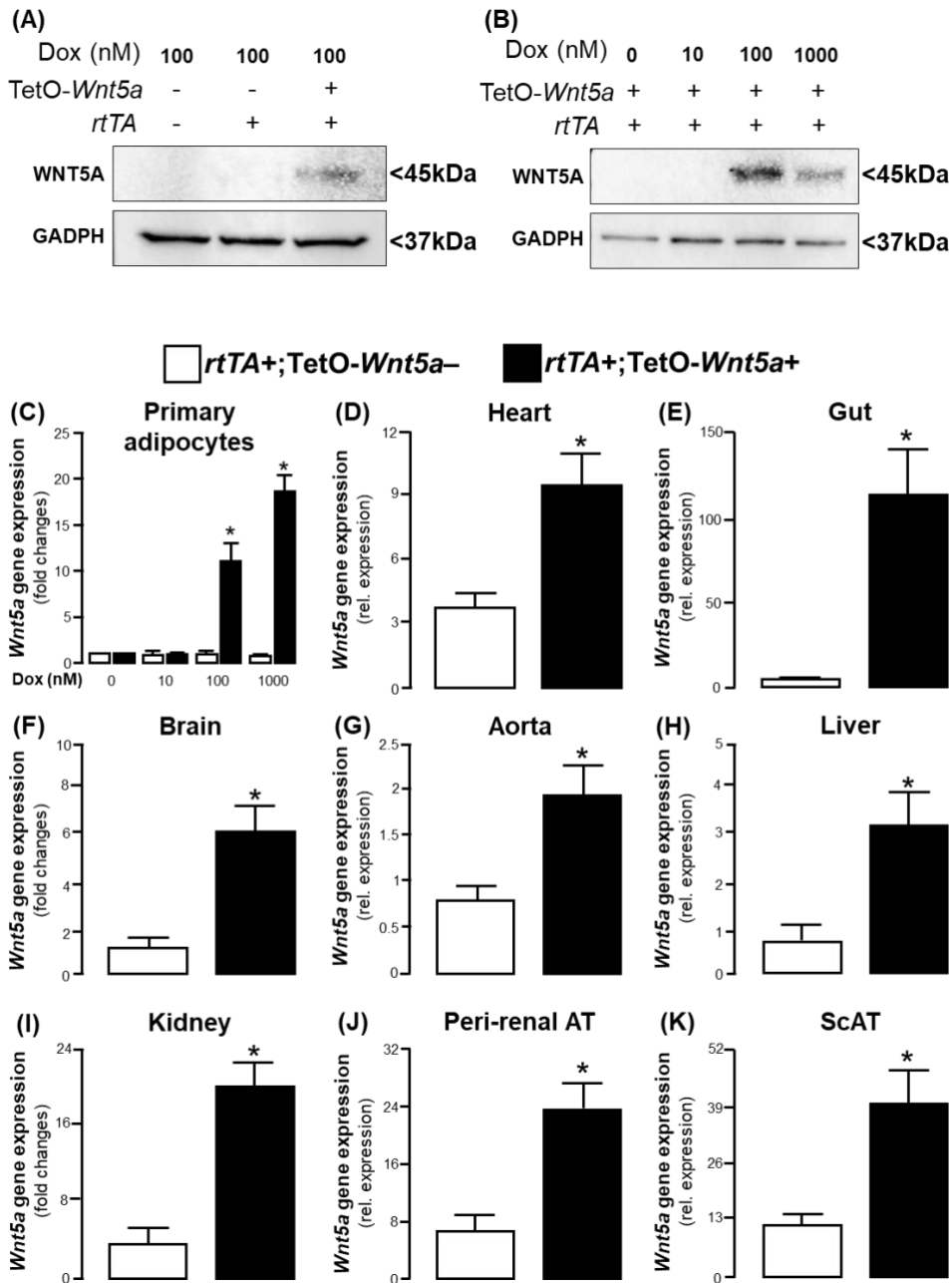
Fig. S5. Phenotyping of the TetO-*Wnt5a rtTA* mouse model. (A) Overexpression of *Wnt5a* in primary adipocytes from TetO transgenic mice following doxycycline 100 nM treatment (n=3); **(B)** Dose-dependent induction of *Wnt5a* overexpression in primary adipocytes from *rtTA*+/TetO-*Wnt5a*+ mice with doxycycline (n = 3); **(C-K)** *Wnt5a* overexpression amplitude in primary adipocytes (n = 3 per group) and a variety of tissues (n = 4-6 per group for all tissues) from TetO transgenic mice. * $P < 0.05$ vs control calculated by Mann Whitney U test (D-K) or unpaired t-test (C). Data presented as mean ± SEM.
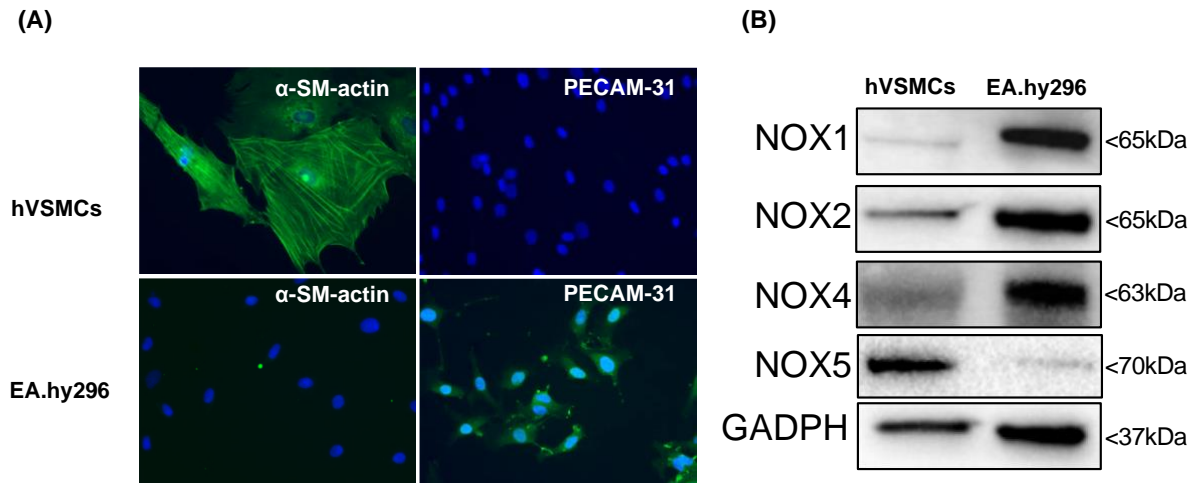
Fig. S6. Phenotyping of isolated primary vascular smooth muscle cells (VSMCs). (A) Validation of vascular smooth muscle cell (VSMC) isolation efficiency by immunofluorescence staining for alpha smooth muscle actin (α-SM-actin) and PECAM-31, an endothelial cell marker (EA.hy296 cells used as endothelial cell marker controls); **(B)** NOX isoform western blotting in primary VSMCs (EA.hy296 cells provided as reference controls).
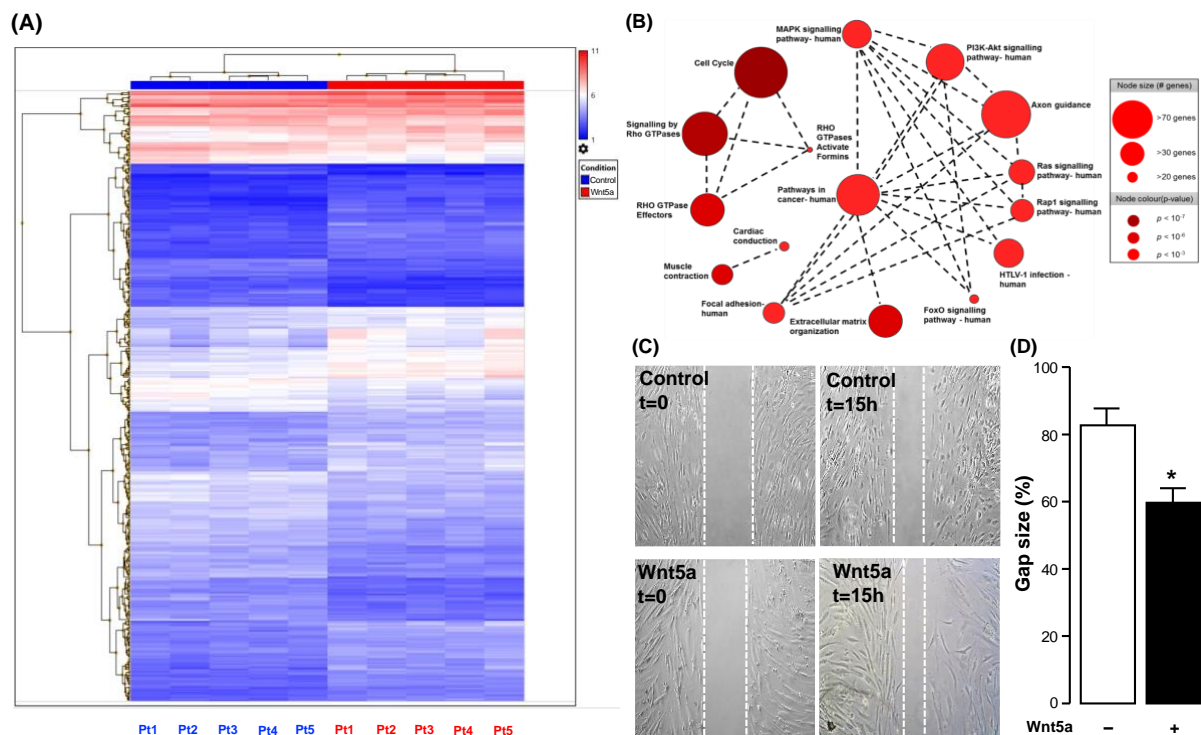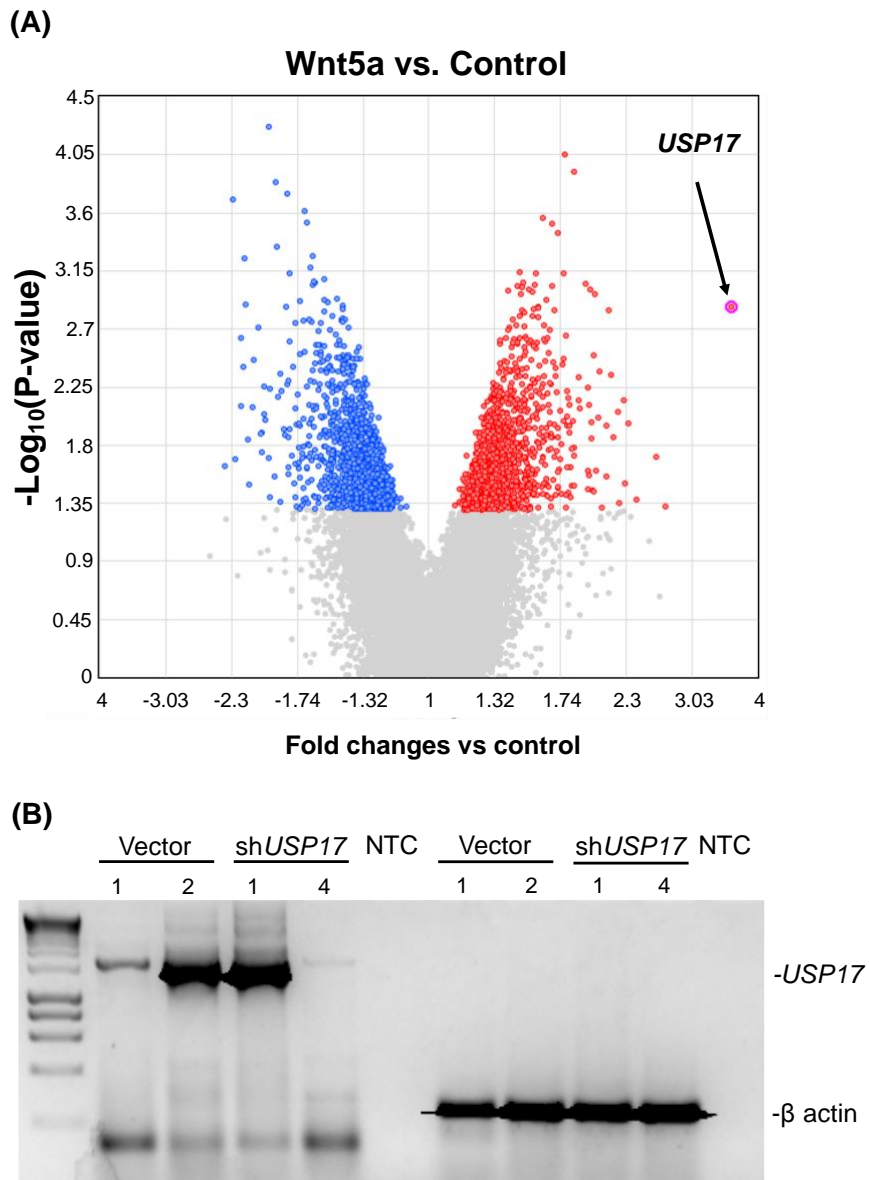
Fig. S7. WNT5A dysregulated genes and pathways and effects on vascular smooth muscle cell (VSMC) migration. (A) Hierarchical clustering of the differentially expressed genes (DEG, fold change >1 or <-1, P-value≤0.05) with and without WNT5A treatment in primary vascular smooth muscle cells (VSMCs) from n = 5 patients. The rows represent the genes and the individual patient samples are shown as columns (1 column per sample). The expression level of each gene (log2 -transformed) is represented as a colour continuously mapped on the colour scale provided. The dendrograms provide some qualitative means of assessing the similarity between genes and between patient samples. **(B)** Pathway enrichment analysis of the set of WNT5A DEGs identified statistically enriched signalling transduction pathways that control several vital cellular processes including cell growth, differentiation, development, apoptosis and migration. **(C-D)** Wound healing assay in WNT5A-treated VSMC (n = 6), data presented as mean ± SEM. * $P < 0.05$ vs control by Wilcoxon signed rank test.
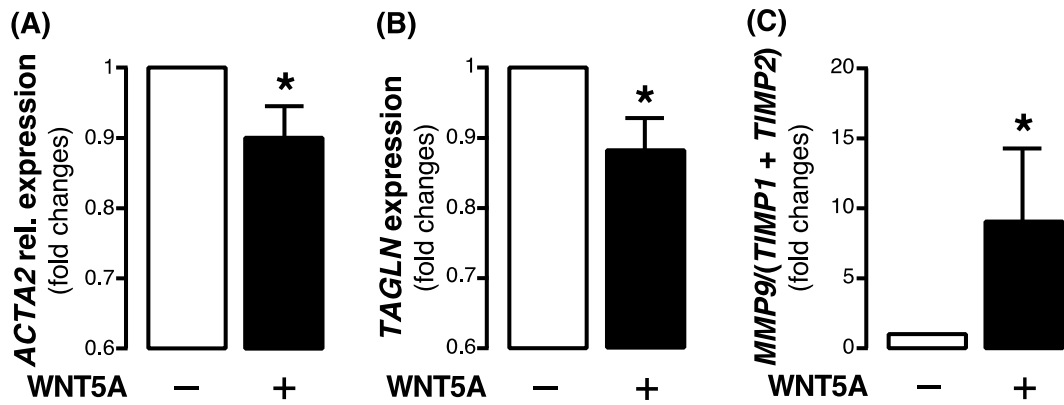
Fig. S8. WNT5A and vascular smooth muscle cell (VSMC) phenotypic switch. (A) A*CTA2* (α2 smooth muscle actin, n = 9 pairs) expression in WNT5A-treated VSMCs; **(B)** *TAGLN* (transgrelin, n = 9 pairs) expression in WNT5A-treated VSMCs; **(C)** Expression of metalloproteinase 9 (*MMP9*, an MMP linked with atherosclerosis progression) relative to its inhibitors *TIMP1 & 2* (tissue inhibitors of metalloproteinases) in WNT5A-treated VSMCs (n = 9 pairs). *$P<0.05$ vs control by Wilcoxon signed-rank tests. Data presented as mean ± SEM.

(A)

Wnt5a vs. Control

USP17

-Log$_{10}$(P-value)

Fold changes vs control

(B)

Vector   sh*USP17* NTC   Vector   sh*USP17* NTC

-*USP17*

-β actin

Fig. S9.   Ubiquitin-specific protease 17 (USP17) as the top hit of WNT5A and USP17 transfection in HeLa cells. (A) Volcano plot of the differential expression of all altered genes upon WNT5A treatment of vascular smooth muscle cells (VSMCs) (n = 5). (B) HeLa cell shUSP17 transfection (successfully transfected clone 4 was passaged and used for downstream *in vitro* treatments); β actin was used as a housekeeping gene. NTC: negative control.
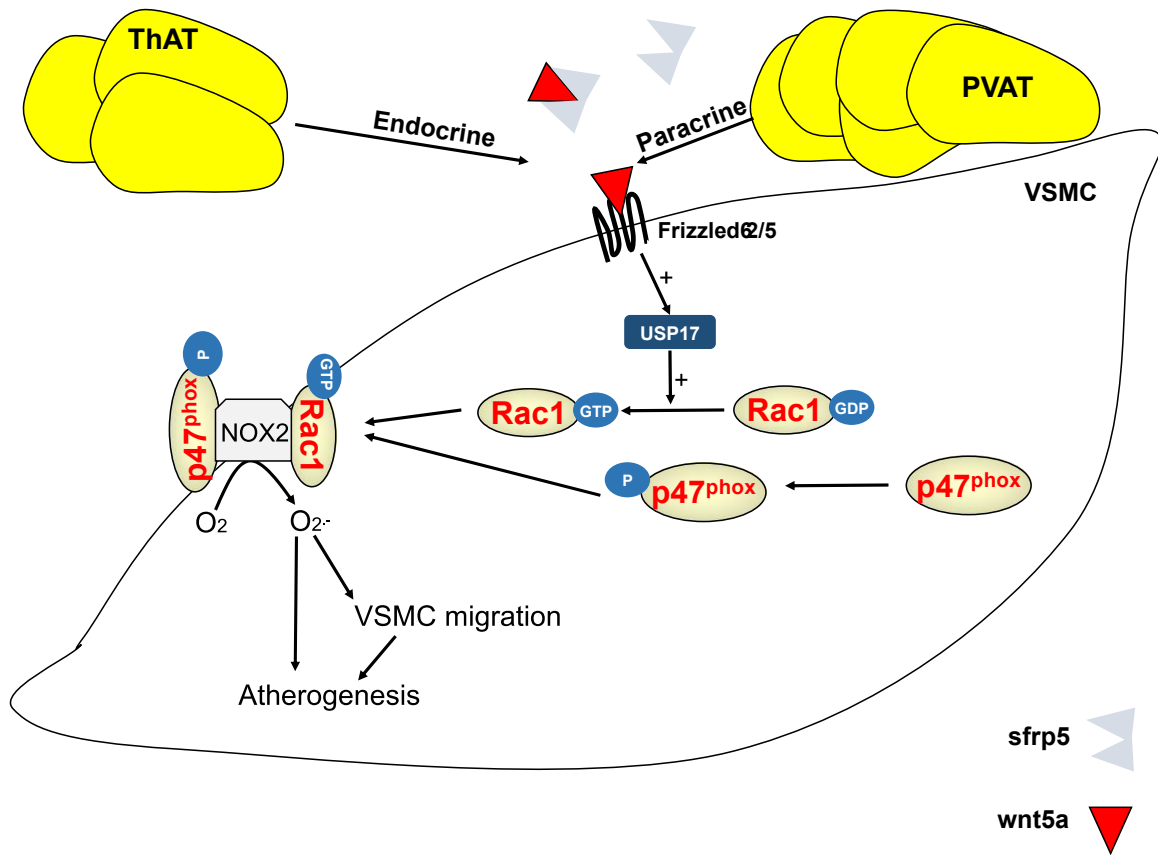
Fig. S10: Schematic diagram with proposed mechanism. WNT5A secreted from perivascular and remote adipose tissue (AT) depots reaches the human vascular wall via paracrine and endocrine routes respectively and exerts Frizzled 2 & 5 receptor-mediated effects depending on its balance with its decoy receptor SFRP5, an effect enhanced in obesity. In the vasculature, WNT5A induces GTP activation of RAC1 and membrane translocation of RAC1 and P47$_{phox}$ subunits of NADPH oxidases isoforms such as NOX2. All these contribute to vascular disease progression. Crucially, we identify the GTPase USP17 as a regulator of WNT5A -mediated RAC1 activation, which may prove to be a rational therapeutic target.

Supplementary tables

Table S1. Demographic characteristics of the study participants. T2DM: Type 2 diabetes mellitus; BMI: Body mass index; ACEi: Angiotensin converting enzyme inhibitor; ARB: Angiotensin receptor blocker; CCB: Calcium channel blocker Continuous variables are presented as mean±SD; **$P < 0.01$ vs CAD, ***$P < 0.001$ vs non-CAD by Chi-square tests.

	Study 1	Study 2		Study 3	Study 4
		Non-CAD	*CAD*		
Participants (n)	1,004	70	70	68	94
Age (years)	66.8±10.1	61.1±6.7	61.3±13	60.4±8.5	66.5±9.4
Males (%)	81.3	42.9	47.1	39.7	83.0
Hypertension (%)	70.6	22.9	78.6***	27.9	71.3
Hyperlipidaemia (%)	87.1	27.1	68.6***	44.1	89.4
T2DM (%)	23.5	2.9	24.3***	36.8	21.3
Smoking					
Active (%)	14.9	4.3	15.7*	6.6	8.5
Past (%)	49.8	44.3	44.3	32.8	46.8
BMI (kg/m2)	28.0±4.6	28.3±5.5	28.4±3.8	28. 1±5.5	28.7±4.2
Medication					
Antiplatelet (%)	73.1	15.7	90.0***	18.0	87.4
ACEi/ARBs (%)	62.3	21.4	77.1***	36.1	60.0
Statins (%)	78.2	22.9	68.6***	41.0	89.5
β blocker (%)	65.2	24.3	70.0***	23.0	75.8
CCB (%)	23.9	14.3	27.1	13.1	20.0
Insulin (%)	13.3	0.0	10.0**	0.0	5.3
Oral hypoglycaemic (%)	17.5	2.9	10.0	11.5	18.9

Table S2. Demographic characteristics of study 1 participants per body mass index (BMI) group. BMI: Body mass index; T2DM: Type 2 diabetes mellitus; ACEi: Angiotensin converting enzyme inhibitors; ARB: Angiotensin receptor blockers; CCB: Calcium channel blockers; +Mean±SD; BMI information missing from 40 of the patients in Study 1. $*P < 0.05$; $**P < 0.01$; $***P < 0.001$ between the groups by Chi-Square tests

BMI group (+BMI in kg/m$_2$)	≤20 (18.8±0.9)	20.1-24.9 (23.2±1.4)	25-29.9 (27.4±1.4)	30-34.9 (32.0±1.4)	≥35 (38.8±4.3)
Participants (n)	25	217	432	233	57
+Age (years)	67.3±16.8	67.5±10.9	67.5±9.5	65.5±9.8	65.3±9.7
Males (%)	64.0	83.9	82.2	78.5	78.9
Hypertension (%)***	58.3	61.8	70.1	76.4	89.3
Hyperlipidaemia (%)	50.0	53.0	49.2	60.5	52.9
T2DM (%)*	20	17.2	21.7	28.8	33.9
Smoking					
Active (%)	9.1	15.9	13.9	16.4	16.4
Past (%)	31.8	42.5	52.4	54.5	54.5
Medication					
Antiplatelet (%)	60.0/8.0	73.5/31.8	73.7/28.9	74.6/28.0	73.2/30.4
ACEi/ARBs (%)	36.0/29.2	50.2/6.2	46.1/14.1	49.4/18.5	51.8/23.2
Statins (%)	68.0	79.1	76.5	81.1	76.8
βblocker (%)**	52.0	67.3	64.2	66.1	64.3
CCB (%)*	16.0	18.0	22.8	30.0	30.4
Insulin (%)**	5.0	2.5	5.0	9.0	14.3
Oral hypoglycaemic (%)**	10.0	10.9	16.2	21.9	26.8

.

Table S3. Multivariate linear regression models of calcified plaque progression and new-onset calcification. Bstand: Standardised linear regression beta (β) coefficient.

Calcified plaque progression		
Variable	**Bstand**	***P***
Plasma WNT5A	***0.242***	***0.047***
Age (per decade of years)	0.191	0.115
Male sex	0.144	0.234
New onset calcification		
Variable	**Bstand**	**P**
Plasma WNT5A	***0.367***	***0.030***
Age (per decade of years)	– 0.069	0.666
Male sex	0.087	0.592

Table S4. Multivariate linear regression models of arterial NADPH-stimulated superoxide (O$_2$.-) production. Bstand: Standardised beta (β) coefficient; PVAT: Perivascular adipose tissue; BMI: Body mass index.

NADPH-stimulated O$_2$.-		
Variable	**Bstand**	*P*
PVAT *WNT5A/SFRP5* ratio	*0.362*	*0.039**
BMI classification	0.316	0.069
Diabetes	0.039	0.817
Smoking	-0.159	0.415
Sex	-0.086	0.650
Age	-0.025	0.885